

**Quality-by-Design inspired formulation of conjugated
polymer nanoparticles as contrast agents and the
assessment of optical imaging performance and
biodistribution**

Kumulative Dissertation

zur Erlangung des
Doktorgrades der Naturwissenschaften (Dr. rer. nat.)

der

Naturwissenschaftlichen Fakultät I
– Biowissenschaften –

der Martin-Luther-Universität
Halle-Wittenberg,

vorgelegt

von Herrn Paul Robert Neumann

geb. am 08.04.1990 in Merseburg

Gutachter:

Prof. Dr. Lea Ann Dailey

Prof. Dr. Karsten Mäder

Prof. Dr. Alexander Kühne

Verteidigung am 15.12.2021 in Halle (Saale)

Table of Contents

TABLE OF CONTENTS	I
LIST OF FIGURES	III
LIST OF TABLES	IV
LIST OF ABBRIVIATIONS	V
1 INTRODUCTION	1
1.1 BIOMEDICAL IMAGING	1
1.1.1 X-RAY	3
1.1.2 X-RAY COMPUTED TOMOGRAPHY	3
1.1.3 POSITRON EMISSION TOMOGRAPHY AND SINGLE PHOTON EMISSION COMPUTED TOMOGRAPHY	3
1.1.4 MAGNETIC RESONANCE IMAGING	4
1.1.5 SONOGRAPHY	4
1.1.6 OPTICAL IMAGING MODALITIES	4
1.2 CONTRAST AGENTS IN BIOMEDICAL IMAGING	9
1.2.1 X-RAY CONTRAST AGENTS	9
1.2.2 MRI CONTRAST AGENTS	9
1.2.3 PET AND SPECT CONTRAST AGENTS	9
1.2.4 SONOGRAPHY CONTRAST AGENTS	10
1.2.5 CURRENT DEVELOPMENTS	10
1.2.6 OPTICAL IMAGING CONTRAST AGENTS	10
1.2.7 CURRENT DEVELOPMENTS	11
1.3 π-CONJUGATED POLYMERS	12
1.3.1 PCPDTBT	15
1.3.2 P4	16
1.4 QUALITY BY DESIGN INSPIRED APPROACH	18
1.4.1 QUALITY BY DESIGN INSPIRED APPROACHES IN ACADEMIC RESEARCH	22
1.4.2 TARGET PRODUCT PROFILE FOR THE CPNs INVESTIGATED IN THE CURRENT STUDY	22
1.5 CPN FORMULATION STRATEGIES	24
2 AIM OF THE PROJECT	28
3 CUMULATIVE PART	30
3.1 GENERAL INFORMATION ON SCIENTIFIC JOURNALS	30
3.2 ITEMIZATION OF OWN CONTRIBUTION	31
3.3 PUBLICATION I	33
3.4 PUBLICATION II	47
3.5 PUBLICATION III	76
4 GENERAL DISCUSSION	98
4.1 QBD INSPIRED CPN RESEARCH	98
4.2 THE IMPACT OF NANOPARTICLE ARCHITECTURE AND COMPOSITION ON CP OPTICAL PROPERTIES	99
4.3 PLQY IS NOT PREDICTIVE OF FLUORESCENCE IMAGING PERFORMANCE IN A PHANTOM MOUSE AND IN VIVO MOUSE MODEL	101
4.4 THE IMPACT OF CPN ARCHITECTURE ON PA IMAGING PERFORMANCE IN A PHANTOM AND IN VIVO MOUSE MODEL	102

4.5 PA AND B-MODE CONTRAST ENHANCEMENT MECHANISMS	104
5 OUTLOOK AND PERSPECTIVES	105
5.1 FURTHER DEVELOPMENTS OF CPN TECHNOLOGY	105
5.1.1 PCPDTBT-RIBONUCLEASE A CONJUGATES FOR PDT AND PTT	105
5.1.2 PCPDTBT-BROMELAIN CONJUGATES FOR PTT	106
5.2 BARRIERS TO CLINICAL TRANSLATION AND FUTURE WORK	106
5.2.1 FUTURE WORK	107
6 SUMMARY	109
7 REFERENCES	112
8 APPENDIX	124

List of figures

Figure 1: Number of cases of diagnostic imaging of different modalities in Germany 2018....	1
Figure 2: A representation of the electromagnetic spectrum	2
Figure 3: Interactions between light and physiological tissue components and absorption spectra of selected endogenous contrast agents.....	5
Figure 4: Basic set-up and principles of fluorescence imaging with the IVIS Spectrum.....	7
Figure 5: Basic set-up of the LAZR photoacoustic imaging system (A). The principle of the photoacoustic effect	8
Figure 6: Molecular orbital overlap in an alternating copolymer linkage	14
Figure 7: Chemical structure of (PCPDTBT).....	15
Figure 8: Chemical structure of borylated (PF8-BT), namely P4	16
Figure 9: Molecular energy levels of unborylated F8-BT and fully borylated F8-BT	17
Figure 10: UV-vis absorbance and emission of PF8-BT and borylated polymers P1-P4	17
Figure 11: Main elements of the Quality by Design concept	19
Figure 12: QbD interdependencies	21
Figure 13: Blood vessel with vascularized tumor and administered CPN.....	24
Figure 14: Different CPN architectures	26
Figure 15: PLQY and maximum emission peaks of CPN formulations.....	101
Figure 16: Time-dependent B-mode and PA signal of the CPNs	103

List of tables

Table 1: General QTTP for CPN	23
Table 2: General information on scientific journals.	30
Table 3: Specification of the percentage of own contribution to the publications.....	31

List of abbreviations

5-ALA	5-aminolevulinic acid
BBT	Benzobisthiadiazole
BET	Bacterial endotoxins test
BT	Benzothiadiazole
CFU	Colony forming unit
cGMP	Current good manufacturing practice
CMA	Critical material attributes
CP	Conjugated polymer
CPDT	Cyclopentadithiophene
CPN	Conjugated polymer nanoparticles
CPP	Critical process parameters
CQA	Critical quality attributed
CT	Computed tomography
DNA	Deoxyribonucleic acid
DoE	Design of experiments
DOPC	1,2-dioctanoyl-sn-glycero-3-phosphocholine
DOPE	1,2-dioctanoyl-sn-glycero-3-phosphoethanolamine
DPPC	1,2-dipalmitoyl-sn-glycero-3-phosphocholine
DPPE	1,2-dipalmitoyl-sn-glycero-3-phosphoethanolamine
DSPE	1,2-distearoyl-sn-glycero-3 phosphoethanolamine
EM	Electromagnetic
EPR	Enhanced permeability and retention
FDA	Food and drug administration
FGS	Fluorescence image-guided surgery
FMEA	Failure mode and effects analysis
FR	Far red
GFP	Green fluorescent protein
HbO ₂	Oxyhemoglobin
HbR	Deoxyhemoglobin
HOMO	Highest occupied molecular orbital
ICG	Indocyanine green

ICH	The international council for harmonisation of technical requirements for pharmaceuticals for Human use
IR	Infrared
ISO	International organization for standardization
LNC	Lipid nanocapsules
LUMO	Lowest unoccupied molecular orbital
MbO ₂	Oxy-myoglobin
MbR	Reduced myoglobin
MCT	Midchain triglyceride
MRI	Magnetic resonance imaging
MTT	3-(4,5-dimethylthiazol-2-yl)-2,5-diphenyltetrazolium bromide
NBCD	Non-biological complex drugs
NIR	Near infrared
NP	Nanoparticle
OCT	Optical coherence tomography
OLED	Organic-light emitting diodes
OSPE	Organic semiconducting pro-nanoenzyme
PA	Photoacoustic
PAI	Photoacoustic imaging
PCPDTBT	Poly[2,6-(4,4-bis-(2-ethylhexyl)-4H-cyclopenta [2,1-b;3,4-b]dithiophene)-alt-4,7(2,1,3-benzothiadiazole)]
PDI	Polydispersity index
PDT	Photodynamic therapy
PEG	Polyethylene glycol
PET	Positron emission tomography
PF8-BT	Poly(9,9-dioctylfluorene-alt-benzothiadiazole)
PLGA	Poly(lactic-co-glycolic acid)
PLQY	Photoluminescence quantum yield
PPV	Polyphenylenevinylene
PTT	Photothermal therapy
QbD	Quality by design
Qdot	Quantum dots
QTTP	Quality target product profile
RNA	Ribonucleic acid

ROS	Reactive oxygen species
SBR	Signal background ratio
SPECT	Single photon emission computed tomography
THF	Tetrahydrofuran
TPP	Target product profile
UV	Ultra violet
WAX	Wide-angle X-ray scattering

1 Introduction

1.1 Biomedical imaging

Biomedical imaging allows us to look deep into living subjects, opening up enormous possibilities of visualization. Using this non-invasive technique, anatomical features and physiological processes can be depicted. It can provide vital information for the detection and monitoring of disease progression and is used to support medical interventions and to monitor organ and tissue functions¹⁻⁴. A variety of imaging techniques are currently in clinical or research use (Figure 1).

Diagnostic imaging in hospital 2018 (inpatients)

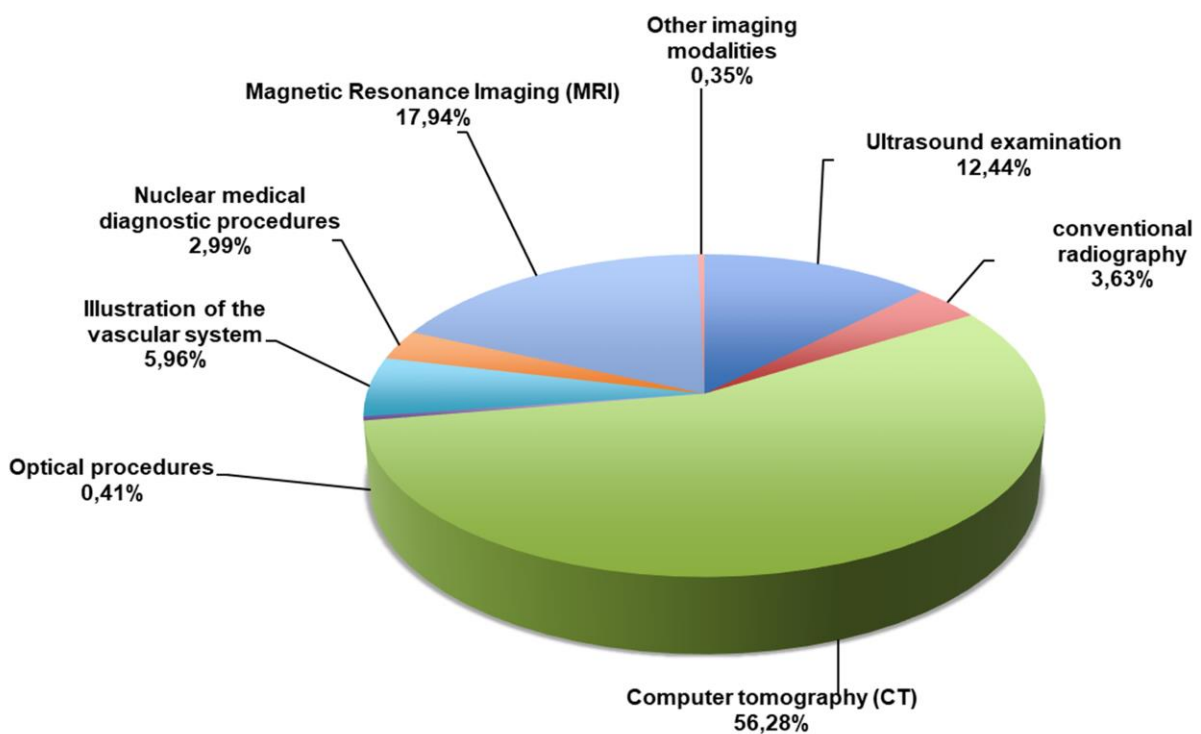


Figure 1: Number of cases of diagnostic imaging of different modalities in Germany 2018 related to hospitalized patients⁵.

Many of these are based on electromagnetic (EM) radiation³. EM radiation encompasses an enormous range of wavelengths and frequencies. This range is commonly referred to as the electromagnetic spectrum. The EM spectrum is typically divided into seven ranges, in order of decreasing wavelength and increasing energy

and frequency (Figure 2). The part of the EM spectrum between 400 - 700 nm that can be perceived by the human eye is called visible light⁶. To be able to explain all phenomena of EM radiation, both the apparent waves and particle properties are considered, which is referred to as wave-particle duality⁷⁻⁹. According to quantum mechanical theories, these particles, called photons, are uncharged elementary particles¹⁰.

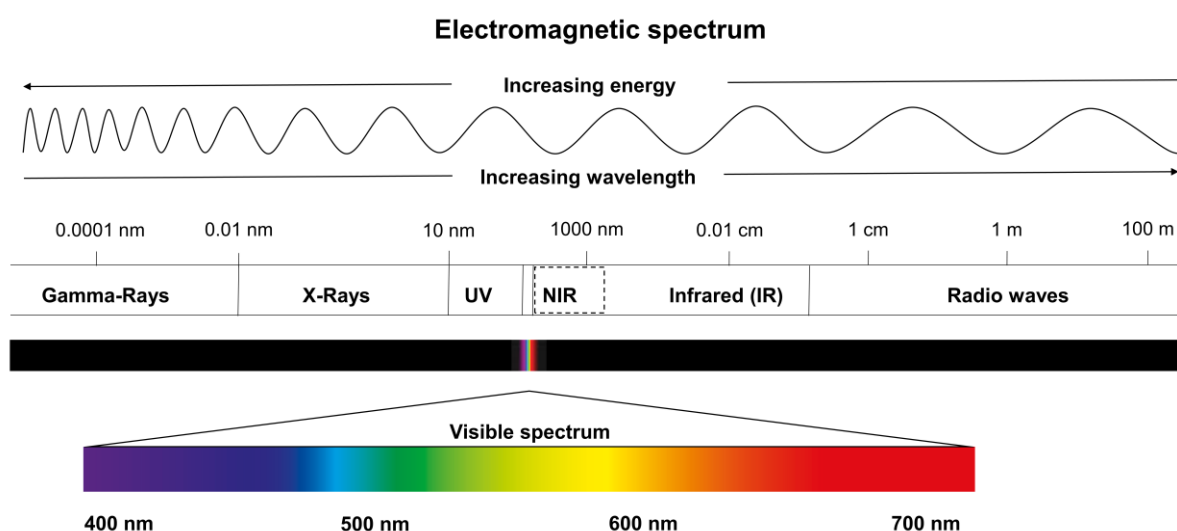


Figure 2: A representation of the electromagnetic spectrum, it shows the different types of electromagnetic radiation and the corresponding wavelength range, with particular consideration of optically visible light. It further shows the relationship between energy and wavelength over the spectral range.

Molecules can absorb EM radiation. Depending on the energy of the radiation there are different changes in the molecule. For example, when absorbing low-energy radiation (e.g. microwaves), there are only transitions from a rotational state to an energetically higher rotational state within the same vibration level. If the absorbed energy is large enough (e.g. near infrared radiation), transitions to energetically higher vibration states within the same electron level occur in addition to the rotational transitions. With the absorption of visible light and UV radiation, molecules are supplied with so much energy that in addition to rotational and vibrational transitions, transitions between electron levels are possible. The absorbed energy can be released by the molecules in the form of radiation (photon emission) or non-radiative processes (vibration, rotation), which both return excited molecules to their ground state^{9,11}.

1.1.1 X-ray

Photons of very high energy, e.g. X-ray can easily penetrate tissues¹². The disadvantage in biomedical imaging is their ionizing effect on molecules, since photons in this frequency range have the necessary energy to remove electrons from atoms¹². Uncontrolled exposure to ionizing radiation can, through a sequence of different reactions, lead to harmful reactive oxygen species (ROS), break chemical bonds and thus cause lasting damage to the intactness of biomolecules in organisms and therefore have carcinogenic effects¹³.

The most commonly used imaging methods in clinical practice (Figure 1) are based on X-rays, e.g. conventional X-rays or X-ray computer tomography (CT)^{6,14}. The radiation generated in an X-ray tube is partially absorbed by the tissue as it passes through the body. On the other side of the body, a detector or film captures the attenuated X-rays, producing a two-dimensional X-ray image¹⁵.

1.1.2 X-ray computed tomography

In contrast, in computed tomography, both the X-ray tube and the detector rotate around the patient's body during the imaging process. Several thousand sectional views of the patient's body are generated per rotation and cross-sectional images are made from these. From these data, three-dimensional images and views from different angles can be generated¹⁶.

1.1.3 Positron emission tomography and single photon emission computed tomography

Molecular imaging offers a whole range of procedures that make it possible to depict biological processes in the metabolism of body cells. For this purpose, small amounts of radioactive substances are administered to the patient. Ultimately, positron emission tomography (PET) and single photon emission computed tomography (SPECT) detect gamma rays, with the difference that these are emitted directly by a radiopharmakon in SPECT and in PET indirectly¹⁷ through the annihilation of elementary particles. A radionucleotide administered for PET emits positrons during decay, which reacts with an electron from the environment, thereby producing gamma photons that are emitted in two opposite directions. In PET and SPECT, the gamma photons hit scintillation crystals and generate light flashes that can be measured and converted into electronic pulses from which images can be generated¹⁸. Furthermore, PET or SPECT imaging

can be combined with images generated by computed tomography (CT) or magnetic resonance imaging (MRI). By superimposing the images from different modalities, the structures and functions of the examined tissue can be displayed in addition to e.g. metabolic processes¹⁹.

1.1.4 Magnetic resonance imaging

MRI is not based on the use of ionising radiation but rather uses radio waves in combination with strong magnetic fields. The hydrogen atoms in the body align themselves in a defined way following application of a magnetic field and are then deflected in their original direction by a high-frequency alternating field in the radiofrequency range, which causes a proton to undergo a certain movement (precession)²⁰. This movement generates a measurable voltage which is detected and converted into an image. An essential basis for the image contrast is the proton density and different relaxation times of the precessing protons of different tissue types after switching off the high-frequency alternating field²¹.

1.1.5 Sonography

Ultrasound (US) or sonography is a diagnostic procedure that is not based on electromagnetic (EM) radiation. This imaging modality does not use ionizing radiation but rather high-frequency sound waves to produce images of internal organs, tissues or blood circulation. The sound waves are directed at the area of the body to be examined and the echoes reflected in the process are recorded²². The well-known black and white contrast (B-mode image) is due to the different reflection and scattering (echogenicity) of the sound wave pulses and impedance (sound wave propagation resistance). On the final images, structures that strongly reflect sound waves (i.e. high echogenicity) appear brighter than structures with low reflective properties (i.e. low echogenicity).²³

1.1.6 Optical imaging modalities

Some components of living organisms can efficiently absorb light of various wavelengths (Figure 3 B), from UV radiation (DNA/RNA; collagen; porphyrin; tryptophan) to visible light (oxyhaemoglobin, deoxyhaemoglobin and melanin) and near-infrared radiation (water; lipids)^{24–26} Some of these components emit light as a result of light absorption, a phenomenon called autofluorescence. Autofluorescence

can be used in some cases to illuminate the molecules and structures of interest or even for diagnostic purposes²⁷.

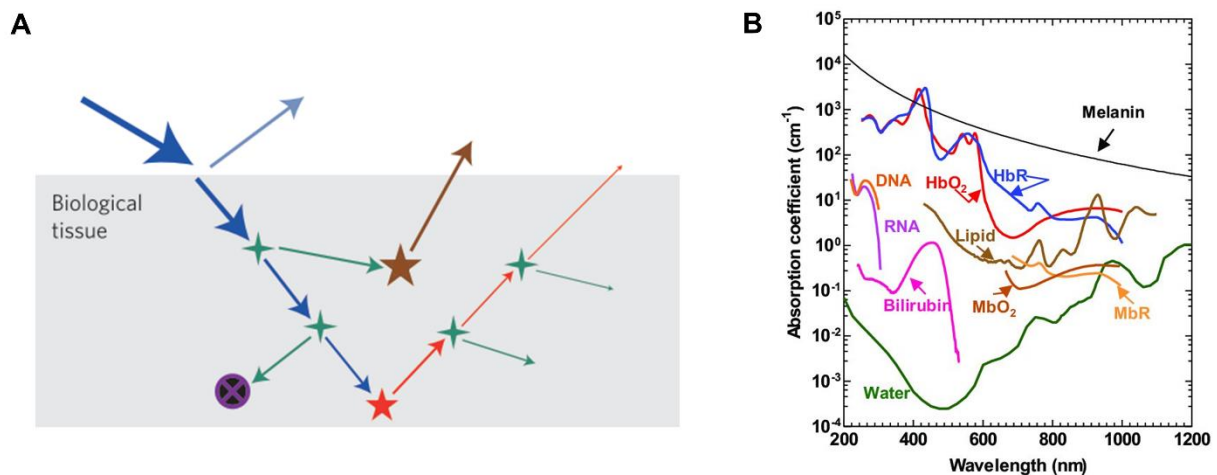


Figure 3: Interactions between light and physiological tissue components due to incident excitation light (blue) (A). Interface reflection (cyan), scattering (green), absorption (black circle with violet cross) and autofluorescence (brown) all contribute to signal loss (fluorescence, red) and noise amplification, reprinted by permission from Springer Nature¹. Absorption spectra of selected endogenous contrast agents in biological tissue at physiological concentrations (B), reprinted by permission from John Wiley and Sons²⁸. Oxy-hemoglobin (HbO₂) and deoxy-hemoglobin (HbR), 150 g/L in blood; lipid, 20% by volume in tissue; water, 80% by volume in tissue; DNA and RNA, 1 g/L in cell nuclei; melanin, 14.3 g/L in medium human skin; reduced myoglobin (MbR) and oxy-myoglobin (MbO₂), 0.5% by mass in skeletal muscle; bilirubin, 12 mg/L in blood.

However, to achieve deep tissue penetration and good spatial resolution, high-energy radiation of the EM spectrum can be used, as already described. Optical imaging techniques can also enable deep tissue penetration and good spatial resolution by using the region of the EM spectrum known as the "transparency window". This describes the wavelength range between 700 - 1300 nm, in this range the endogenous absorption and light scattering of biological tissues and physiological fluids is low²⁹. When UV and visible light interact with tissue, light is scattered by the biological structures (Figure 3 A) as it passes through or is absorbed as described above. The near-infrared range, however, is a range that leads to deeper tissue penetration due to the reduced interaction of radiation of these wavelengths with tissue^{30,31}.

Photographic optical imaging is well known and has been around for about 200 years. It is considered the oldest optical imaging technique for creating images of objects using visible light⁶. The first photograph is dated back to 1826, the "View from the Window at Le Gras" was taken with a camera obscura by the French inventor Nicéphore Niépce³². Modern advances in biomedical optical imaging have resulted in

applications such as microscopy, endoscopy, optical coherence tomography, diffuse reflectance and transillumination imaging and photoacoustic imaging^{6,27}. Optical imaging uses non-ionizing radiation, which includes visible, ultraviolet, and infrared light to interrogate organs and tissues as well as smaller structures including cells or molecules. The wavelengths used in optical imaging produce images without the potential damage that can occur with ionizing radiation, making this imaging option much safer for patients and health care professionals. Since the procedures are also much faster, it can be used for repeated procedures to monitor the progression of the disease or the results of treatment. Although optical imaging is usually much faster, has a higher throughput and can be less expensive compared to other imaging methods (X-ray; CT; MRI), optical imaging is not yet widely used in clinical practice (Figure 1), apart from image-guided endoscopy and optical coherence tomography (OCT).

1.1.6.1 Fluorescence imaging

As briefly mentioned, molecules can absorb photons. The valence electrons of the atoms of these molecules thus reach a higher energy level and are then in an excited state^{24,25}. From this excited state the electron can return to its ground state by emitting light, which is known as photoluminescence³³. Depending on the duration of the glow after the end of excitation, a distinction is made between fluorescence (10^{-12} - 10^{-6} s) and phosphorescence (at least 10^{-3} s)^{9,34}. Compared to absorbed light, the emitted light is shifted towards the longer-wave, lower-energy region of the spectrum, which is called a Stokes shift³³.

Microscopic fluorescence imaging is used to study cellular structures and tissue sections, while whole-body fluorescence imaging is currently used in pre-clinical development, especially in rodent models (Figure 4). Localized fluorescence imaging techniques, such as fluorescence-guided surgery and endoscopy are also used clinically¹⁴. Key challenges in fluorescence imaging comprise tissue absorption, scattering, and autofluorescence, all of which limit penetration depth^{4,35} (Figure 3). Since both tissue absorption and autofluorescence decrease in the far-red (FR) or near-infrared (NIR) wavelength range, imaging in the NIR region is most suitable for in vivo applications^{1,36}.

Fluorescence imaging with the IVIS Spectrum

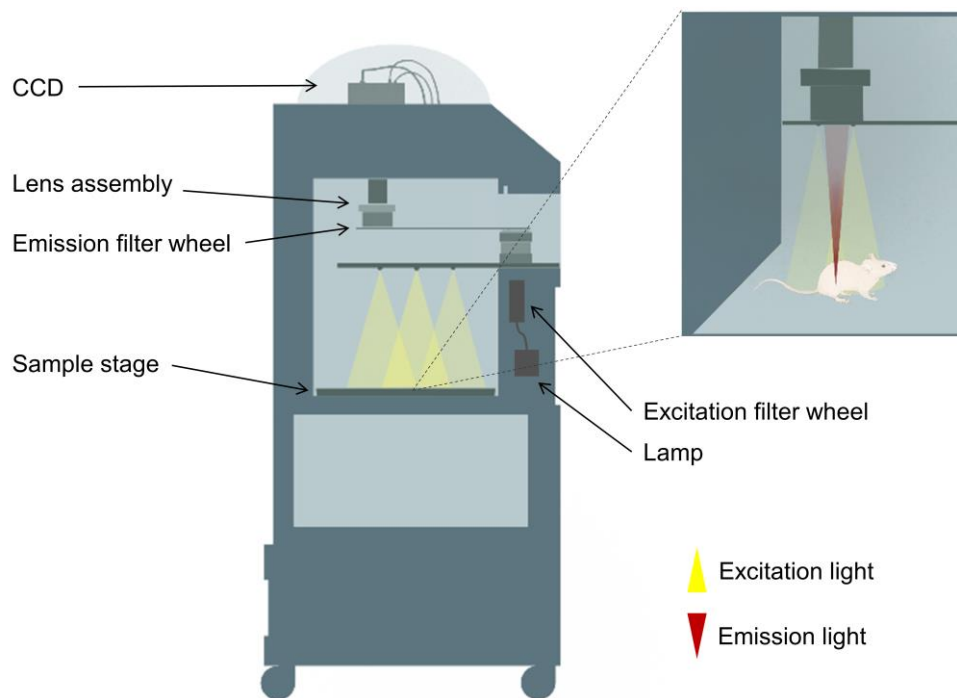


Figure 4: Basic set-up and principles of fluorescence imaging with the IVIS Spectrum according to IVIS Spectrum user's manual.

1.1.6.2 Photoacoustic imaging

At the end of the 19th century Alexander Bell was the first to describe the photoacoustic effect. This is based on the conversion of absorbed light into thermal energy and finally, via thermoplastic effects, into ultrasound³⁷. The light source is a laser that pulses in the nanosecond range, because only when the laser pulse is short the thermal expansion will cause a pressure wave proportional to the locally absorbed energy density generated by the photoacoustic effect (Figure 5 B). These pressure fluctuations (ultrasound) caused by the periodic expansion and contraction can be measured with pressure-sensitive elements such as piezoelectric transducers³⁸. The electrical signals generated by the transducer are amplified, digitized and finally processed into an image by means of computer algorithms²⁷ (Figure 5 A). Photoacoustic imaging is also known as optoacoustic, laser-induced ultrasound or thermoacoustic imaging³⁹.

Photoacoustic imaging

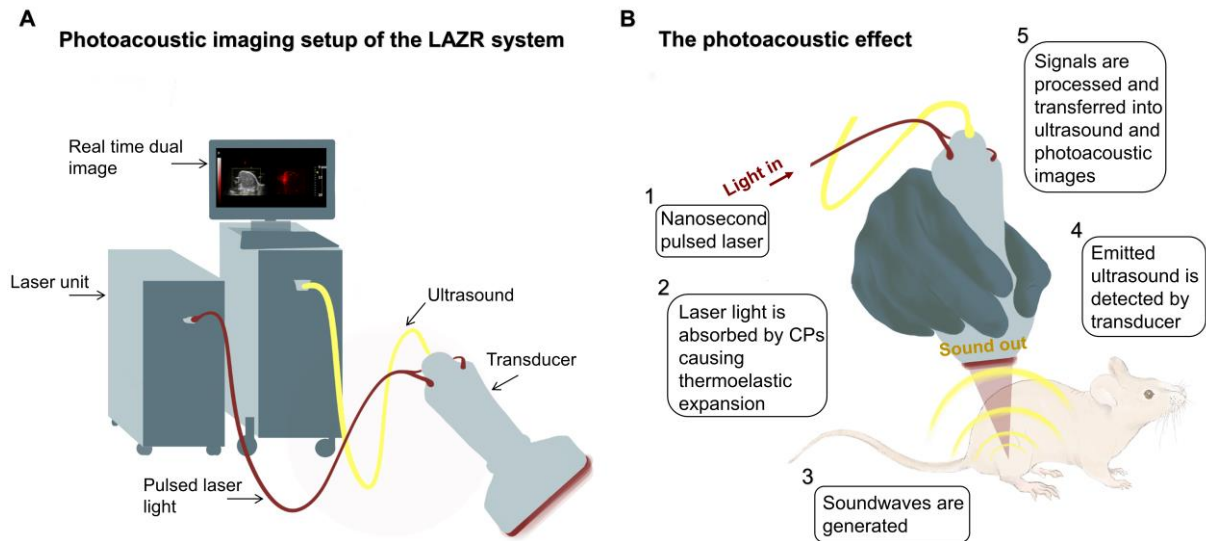


Figure 5: Basic set-up of the LAZR photoacoustic imaging system (A). The principle of the photoacoustic effect (B) according to the website of the manufacturer⁴⁰.

Biological tissues cause strong optical scattering, which ultimately leads to the disadvantages such as low imaging depth and low spatial resolution⁴¹. Since the scattering of the ultrasound signal generated by the photoacoustic effect is much weaker than the optical scattering, photoacoustic imaging offers deeper penetration with better resolution than optical diffuse imaging techniques^{42,43}. PA imaging uses the different light absorption properties of endogenous light absorbing components such as hemoglobin, collagen, lipids and water, which are tissue-specific⁴⁴. Therefore, this technique does not necessarily require exogenous contrast agents for certain applications. For example, oxyhaemoglobin and deoxyhaemoglobin can be differentiated and quantified by means of multi-wavelength measurements²⁷. Measurements of blood oxygen levels is probably the main application of PA imaging so far and has been applied to study vascular biology, brain function, tumor hypoxia, and wound healing⁴⁵. However, the majority of current PA applications can be found in research and preclinical studies. Clinical applications of PA imaging have been recently reported in the fields of breast imaging, rheumatoid arthritis, systemic sclerosis, and carotid artery disease⁴⁶.

1.2 Contrast agents in biomedical imaging

In biomedical imaging, the generation of high-resolution, high-contrast images is desirable because it enables accurate and precise diagnoses. Contrast agents are diagnostic tools used in imaging for better visualization of physiological and pathological structures as well as processes. They are used clinically or at an experimental level in all the techniques mentioned above. The contrast media are classified as medicinal products must therefore meet requirements of efficacy, safety and pharmaceutical quality⁴⁷. However, the guidelines for the development of contrast media mainly focus on radiopharmaceuticals. When developing other types of imaging agents, it is therefore necessary to follow established test packages that have already been published and/or the "Guidance for Industry Developing Medical Imaging Drug and Biological Products Part I Conducting Safety Assessments" in order to meet the requirements for starting clinical studies⁴⁸.

1.2.1 X-ray contrast agents

X-ray contrast media (barium sulfate; derivatives of triiodobenzoic acid) increase the difference in density between the organ to be imaged and the surrounding tissue⁴⁹. Some of the X-ray contrast media can be found in the WHO List of essential medicines⁵⁰.

1.2.2 MRI contrast agents

MRI contrast media (gadolinium and manganese chelate complexes; superparamagnetic iron oxides) shorten the relaxation time of the protons in the vicinity and thus increase the contrast between different structures in the body⁴⁹.

1.2.3 PET and SPECT contrast agents

Radiopharmaceuticals for PET imaging are isotopes (¹⁸F, ¹¹C, ¹⁵O) bound to endogenous metabolic molecules and are thus integrated into the metabolism⁴⁹. When they decay, positrons are created. When a positron encounters an electron, both elementary particles are annihilated, resulting in a pair of annihilation photons (gamma radiation), which move in opposite directions. SPECT contrast agents (e.g. chelated technetium-99m) emit gamma radiation that is measured directly⁵¹.

1.2.4 Sonography contrast agents

Ultrasonic contrast media are gaseous (air, sulfur hexafluoride, perflutrene) echogenicity enhancers on the micrometer scale⁴⁹. These gas contrast agents, compress and oscillate when exposed to ultrasound, the ultrasound backscatter (reflection) of ultrasound waves is thus enhanced, resulting in a sonogram with increased contrast due to the high echogenicity difference⁵².

1.2.5 Current developments

Current exogenous contrast agents have a great value in providing diagnostic information, but they still have certain disadvantages such as short circulation half-lives, non-specific biodistribution, rapid clearance, mild renal toxicity and poor contrast in obese patients²⁰. Research is being conducted on nanoparticles as novel contrast agents, which represent a promising strategy for non-invasive diagnosis with the imaging modalities described above. Some diagnostic nanoparticles for MRI, PET and SPECT have received clinical approval or are currently enrolled in clinical trials⁵¹. Nanoparticles are also the subject of intensive research for other imaging modalities, such as biomedical applications in the emerging field of optical fluorescence and photoacoustic imaging.

1.2.6 Optical imaging contrast agents

1.2.6.1 Fluorescent contrast agents

Endogenous fluorophores are typically irrelevant as a source of optical contrast for this imaging method. However, exogenously administered fluorophores (e.g. dyes, quantum dots, organic polymers), fluorophore precursors like 5-aminolevulinic acid (5-ALA) or genetically engineered fluorescent proteins (e.g. GFP) are used to enhance optical contrast^{35,53}. As the imaging depth is still limited to a few cm⁵⁴, a large scope remains for the further development and improvement of contrast media for this application.

Traditionally in clinical practice, small molecular dyes have dominated as fluorescence contrast agents. The FDA approved NIR-emitting tricyanocyanine dye, indocyanine green (ICG), has been in clinical use since 1959⁵⁵ and is therefore often used as a benchmark fluorophore when developing new optical contrast agents. It has since been used to investigate cardiac physiology, in ophthalmologic angiographic

fluorescence procedures and in tumor diagnostics⁵⁶. Despite its wide use, ICG shows some disadvantages, including degradation in aqueous solution, rapid photobleaching, rapid plasma clearance, nonspecific binding to albumin, lipoproteins, plasma proteins and endothelial cells, as well as concentration-dependent aggregate formation^{57–59}, which changes the optical properties and can detrimentally affect clinical utility. These disadvantages have to be overcome in order to improve diagnostics in patients. Three other small molecule contrast agents (fluorescein, methylene blue and 5-aminolevulinic acid) are approved by the FDA⁵³, however, ICG is the only dye that both absorbs and emits in the NIR range.

1.2.6.2 Photoacoustic contrast agents

In addition to naturally occurring chromophores, exogenous PA contrast agents have been investigated. In general, contrast agents for PA imaging require a high radiation-free relaxation, so the PLQY should be as low as possible⁶⁰. Examples of materials studied include gold nanorods, single-walled carbon nanotubes, organic NIR dyes (e.g. ICG) and π -conjugated polymer nanoparticles (CPN). All these materials can be used to produce even higher contrast images with deeper tissue penetration^{42,61,62}.

1.2.7 Current developments

The pipeline of contrast agents based on dyes for fluorescence image guided surgery is filled with a wide variety of dyes, formulations and targeting mechanisms, some of which have already reached Phase III clinical trials⁵³. However, many of these dyes also have disadvantages, such as a small Stokes shift and rapid photobleaching, which ultimately limits the application methods⁶³.

π -conjugated polymers (CPs) are a relatively new class of material under investigation for uses as in vivo optical contrast agents⁶⁴ for fluorescence and photoacoustic imaging. They show excellent optical properties for this application, such as large Stokes shift, high photostability, sufficient brightness and, compared to quantum dots (Qdots), strongly improved safety and toxicity profiles, since they do not contain heavy metals⁶⁵. Compared to commercially available quantum dots (Qdot 655) and organic dyes such as Alexa Fluor 555 and Rhodamine 6G, some CPN contrast agents showed improved photostability and larger Stokes shifts. The same systems were also shown

to be efficient FR/NIR fluorescence probes for targeted in vivo fluorescence imaging and cancer detection, while exhibiting negligible toxicity⁶⁰

1.3 π -conjugated polymers

π -conjugated polymers (CP) are organic materials, characterized by photo-/electroluminescence due to their chemical structure^{66,67}. For energetic reasons the orbitals of the atoms in these structures overlap and form molecular orbitals. The existing molecular orbitals can be occupied by electrons. The orbital overlap results in chemical bonds, where a distinction is made between sigma (σ) bonds and p (π) bonds. With σ bonds, the orbital overlap results in a rotationally symmetrical bond. π bonds, however, are created when the p orbitals are perpendicular to the plane of the σ bonds and overlap above and below this plane. The property-determining structural feature of π -conjugated polymers are conjugated double bonds along the backbone, i.e. the bonds between the atoms are alternately single and double bonds. Each bond consists of a localized σ bond; these bonds are strong chemical bonds. Double bonds have an additional, π bond to the σ bond. These π bonds are less localized and represent weaker chemical bonds⁶⁸. The overlapping of the p orbitals between the atoms leads to a delocalization of electrons along the entire polymer backbone, allowing the electrons to move freely^{69,70}. The highest with electrons occupied orbital of a molecule (HOMO or π -band) has a lower energy than the lowest unoccupied orbital (LUMO or π^* -band) of a molecule. The difference in energy between HOMO and LUMO is called band gap⁷¹ (Figure 6). By excitation of the electrons within the π band, π - π^* transitions can be enabled, i.e. the band gap between HOMO and LUMO can be overcome. This is also decisive for the useful photoconductive properties of CPs.

The conjugation of a polymer alone, however, is not solely responsible for the semiconducting properties; in addition, charge carriers must be introduced into the material. These can be introduced by so-called dopants. Depending on the dopant introduced, either additional electrons (electron donors) or "holes" (electron acceptors) contribute to conductivity in the polymer⁶⁸. Holes in this sense are positions where electrons are missing. If the hole is filled by an adjacent electron, a new hole is created,

thus enabling charge transport⁶⁸. Semiconductor materials with more "holes" than electrons are called a p-type or (positive) semiconductors because the acceptor density of p-type semiconductors is greater than its donor density. In contrast, n-type (negative) semiconductors contain an excess of electrons for charge transport⁷².

Doped or undoped CPs are useful for a wide range of applications. In the undoped state a large number of CPs show strong photoluminescence in the visible and near infrared range of the spectrum¹⁴. Doping, however, makes it possible to more precisely adjust the desired optoelectric properties. Any structural change made at the polymer also changes the HOMO-LUMO band gap of the electronic transition between π and π^* orbitals, which ultimately defines the color of the emitted light^{71,73}. Thus, if the energy condition is fulfilled, a photon with a certain wavelength can excite an electron in such a way that a transition from the HOMO (π) to the LUMO (π^*) level is made possible⁷³.

Polyaniline is the first reported CP and it was also argued that it is the first fully synthetic polymer⁷⁴. Before the 1960s, it was known by various color-based names (i.e. emeraldine, azurine, aniline black, etc.). Production of polyaniline was of course dependent on the availability of aniline per se. Between 1826 and 1842, several scientists independently reported an oily reaction product based on different raw materials, indigo (*Indigofera tinctoria*), coal tar or nitrobenzene. It was first isolated by Otto Unverdorben through the dry distillation of indigo; Ferdinand Runge discovered it through the distillation of coal tar; Carl Julius Fritzsche isolated it through the distillation of a brown salt obtained through the basic treatment of indigo; and Nikolai Zinin described it after the reduction of nitrobenzene. In 1843, it was shown by August Hoffmann that these reaction products were one and the same substance, aniline, named after anil, an ancient name of the indigo plant. Patents and the commercialization of dyes followed until the next major innovation came in 1862 from the English physician and chemist, Henry Letheby, who was the first to report the electropolymerization of a CP⁷⁵.

However, it was not until the work on the synthesis of polyacetylene in the 1970s, nearly a century later, that the field of CPs attracted renewed scientific attention. Polyacetylene was first synthesized in 1955. However, in 1976 it was observed that the electrical conductivity of polyacetylene can be increased by several orders of

magnitude by doping. This discovery paved the way for applications of CPs in optoelectronic devices, ultimately leading to the award of the Nobel Prize in Chemistry to the three inventors, Alan J. Heeger, Alan G. MacDiarmid, Hideki Shirakawa in 2000^{74,75}.

In addition to polyacetylene, other CPs with different backbone structures have been synthesized, including polypyrroles (1915), polyphenylenes (1949), polyphenylenevinylenes (1969), and polythiophenes (1980). The homopolymers and their corresponding doped systems are now classified as the first generation of CPs⁷⁶. The use of first generation CPs for electroluminescent devices was made possible in the early 1990s with polyphenylenevinylenes (PPV)⁷⁷.

The second generation of CPs⁷⁶ improved on first generation materials through synthesis of donor-acceptor polymers, which reduced the band gap (Figure 6).

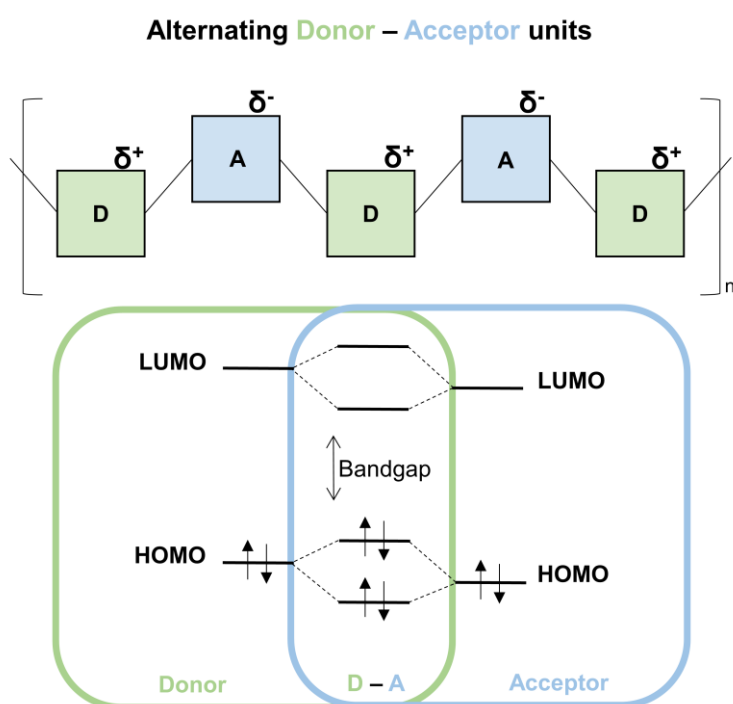


Figure 6: Molecular orbital overlap of an electron rich (Donor: D) and an electron-deficient moiety (Acceptor: A) in an alternating copolymer linkage according to Hildner et al⁷⁶.

The underlying concept is based on the molecular orbital overlap of alternating electron-rich (donor: D) and electron-poor (acceptor: A) conjugated moieties that are incorporated into the polymer backbone. This alternating D-A arrangement is an effective method to reduce the band gap and further improve the optical and electrical

properties of the CPs⁷⁶. Computational modelling of the molecular orbitals of such a compound has shown that the HOMO is mainly located on the electron donor (fluorene) and LUMO is exclusively located on the electron acceptor (benzothiadiazole)⁷⁸.

Second generation CPs are currently used as light sources in various devices such as organic light-emitting diodes (OLEDs)^{79–82}. Further applications include e.g. solar cells⁸³, as corrosion inhibitors⁸⁴, antistatic coating materials⁶⁸, field effect transistors⁷⁶, capacitors, smart windows, high definition fingerprint visualization⁸⁵ and fluorescent biosensors⁸⁶. Two second generation CPs have been chosen for study in this work. Their chemical structure and properties are described in the following sections.

1.3.1 PCPDTBT

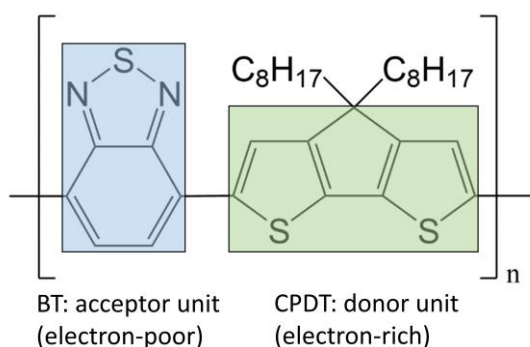


Figure 7: Chemical structure of poly[2,6-(4,4-bis-(2-ethylhexyl)-4H-cyclopenta [2,1-b;3,4-b']dithiophene)-alt-4,7(2,1,3-benzothiadiazole)] (PCPDTBT). In the structural formula electron-rich fluorene (CPDT) and electron-poor benzothiadiazole (BT) unit are highlighted.

PCPDTBT (Figure 7), *poly[2,6-(4,4-bis-(2-ethylhexyl)-4H-cyclopenta [2,1-b;3,4-b']dithiophene)-alt-4,7(2,1,3-benzothiadiazole)]* is a CP comprised of alternating cyclopentadithiophene (CPDT) electron-donor units (D) and benzothiadiazole (BT) electron-poor acceptor units (A), which enable intramolecular charge transfer^{87,88}. Although the bulky side groups of the CP are not directly involved in charge transport via the polymer backbone, their influence on the polymer configuration can also influence charge transport and thus the optical properties^{89,90}. Originally developed in 2006 for photovoltaic applications, PCPDTBT shows near-infrared absorbance/emission and photoacoustic properties⁹¹, which makes this polymer suitable for biomedical imaging and photothermal ablation⁹². PCPDTBT is one of the most widely studied p-type semiconductors⁷⁶.

1.3.2 P4

The simple process of electrophilic C-H-borylation was used to modify BT-containing polymers to create a completely new family of FR/NIR-emitting CP. The electrophilic C-H borylation of polyfluorene-benzothiadiazoles (PF8-BT) resulted in CPs with FR/NIR absorption and emission profiles. This C-H functionalization methodology and the percentage of borylated F8-BT units can be simply controlled by varying the molar equivalents of BCl_3 used with respect to the repeat units. This synthesis carried out by our cooperation partners resulted in partially borylated P1- P3 (10, 15 and 25% borylation) and fully borylated PF8-BT, which is called P4 (Figure 8). The fully borylated version, P4 was used in this study because of its excellent optical properties. P4 consists of a donor-acceptor (D-A) π -conjugated system.

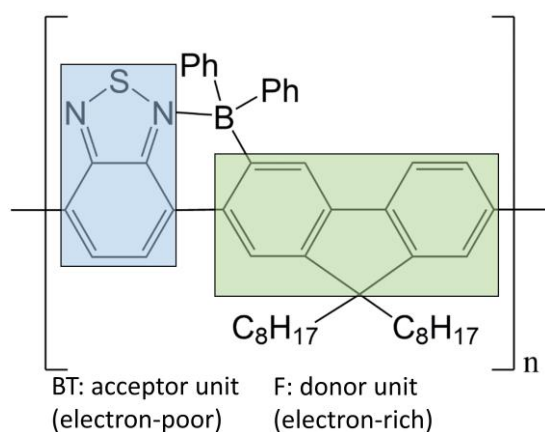


Figure 8: Chemical structure of borylated poly(9,9-dioctylfluorene-alt-benzothiadiazole) (PF8-BT), namely P4. In the structural formula electron-rich fluorene (F) and electron-poor benzothiadiazole (BT) unit are highlighted.

By adding boron to PF8-BT, the acceptor LUMO energy level could be lowered, and additionally the HOMO energy level could be increased due to the inductive effect of the 4-coordinated boron. Not only did this brought the HOMO-LUMO energy levels closer to each other, thus reducing the band gap from 2.57 to 1.94 eV⁹³ (Figure 9).

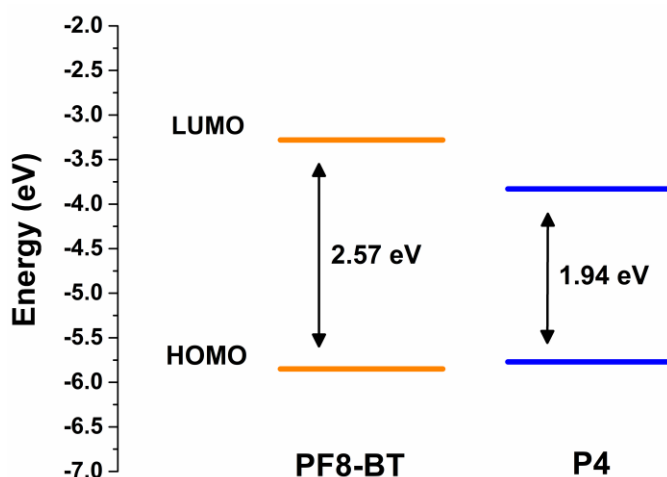


Figure 9: Molecular energy levels of unborylated F8-BT and fully borylated F8-BT, namely P4.

The borylation furthermore locked the donor and acceptor in a coplanar geometry. The borylation modifies the intermolecular packing of the polymer, as the additional bonds prevent monomer twisting. This reduction in rotational degrees of freedom leads to better communication along the conjugated system. The resulting higher coplanarity of the polymer maximizes the extended π conjugation, which may ultimately lead to a further reduction of the band gap⁹⁴. Increasing the fraction of borylated PF8-BT units results in a successive shift of the absorbance maximum from ~ 450 nm (non-borylated PF8-BT) to ~ 610 nm (100% borylation), the emission maximum from 527 nm to ~ 700 nm (Figure 10) and a quantum yield for the fully borylated PF8-BT of $\sim 12\%$ when measured in toluene solution⁹³.

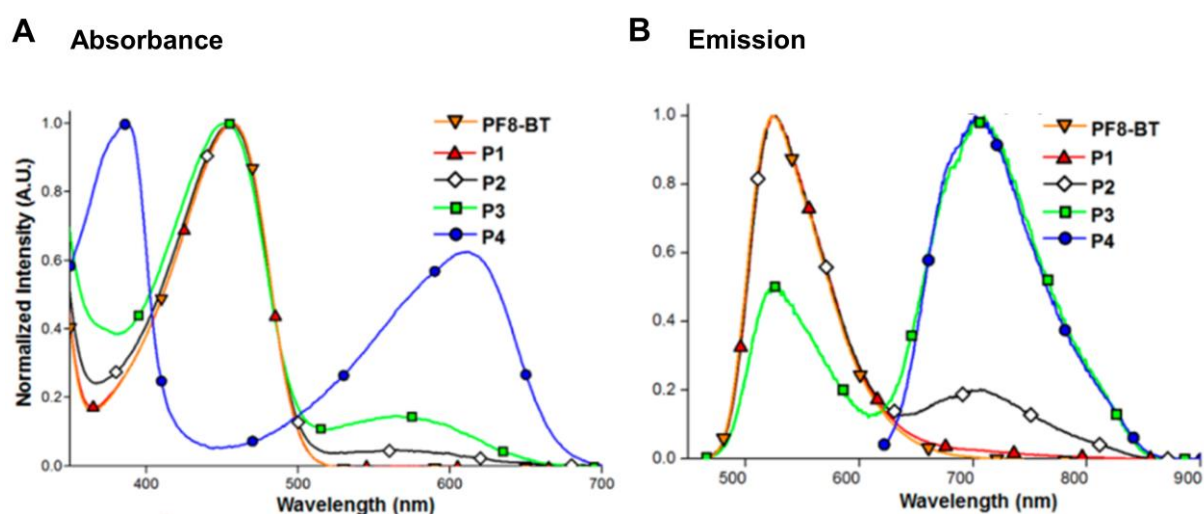


Figure 10: UV-vis absorbance (A) and emission (B) of PF8-BT and borylated polymers P1-P4⁹³.

Looking at the class of second generation alternating donor-acceptor copolymers, p-type copolymers containing benzothiadiazole (e.g. PCPDTBT) are among the most studied materials⁷⁶. P4, on the other hand, was not patented until 2015 together with other reduced band gap borylated compounds⁹⁴. Due to the inherent lipophilicity of CP, they must first be processed into nanoparticles to ensure colloidal stability and biocompatibility when used clinically⁹⁵. Due to an inherent complexity in composition, the polymeric nanodiagnostics investigated in this study would be classified as non-biological complex drugs (NBCD) and therefore a structured production design strategy would be beneficial⁹⁶. An approach inspired by Quality by Design (QbD) was applied in publications II and III to identify and characterize critical quality parameters that play a crucial role for the potential intravenous application of CPN nanodiagnostics.

1.4 Quality by design inspired approach

Quality has manifold definitions, for example it can be understood as excellence, value, conformity to specifications, conformity to requirements, fitness for purpose, loss prevention and meeting and/or exceeding customer expectations⁹⁷. Quality gurus such as Philip Bayard Crosby, Joseph M. Juran and W. Edwards Deming began to shape the foundations and establishment of quality management systems, which were first applied in the steel and automotive industries before also finding application in the pharmaceutical industry. Until the uncovering of the serious and dramatic undesirable side effects of Elixir Sulfanilamide (1937) and thalidomide (1957), the pharmaceutical market was minimally regulated⁹⁸. As a result of these tragedies, a number of regulations were successively introduced. However, the modern era in terms of product quality in the pharmaceutical industry did not really begin until 2004 with a concept paper entitled "Pharmaceutical cGMP for 21st Century". Subsequently, the ICH established basic regulatory guidelines, namely Q8 (Pharmaceutical Development), Q9 (Quality Risk Management) and Q10 (Pharmaceutical Quality Systems), which in combination form the basis for the quality by design concept for the production of high-quality medicinal products. The term 'Quality by Design' was first used by Juran in 1985, when the first draft of his book was made available to some industry representatives; it was made available to the wider public with its publication

in 1992⁹⁹. The fact that increased testing does not necessarily improve product quality led to the philosophy: "quality cannot be tested into products but it should be built in or should be designed". According to ICH Q8 (R2), QbD is "a systematic approach to drug development that emphasizes the need to start with predefined goals and understand the product and process based on sound science and quality risk management"¹⁰⁰. Thus, this philosophy can be seen as an experimental design philosophy that emphasizes the value of thorough intellectual planning before starting laboratory studies. But that's not all, QbD principles extend beyond development into the product lifecycle, providing a solid framework for the transfer of product knowledge and process understanding from drug development to commercial manufacturing processes, as well as for changes and optimizations after the development phase¹⁰¹. The main elements of this concept are shown in simplified form in Figure 11.

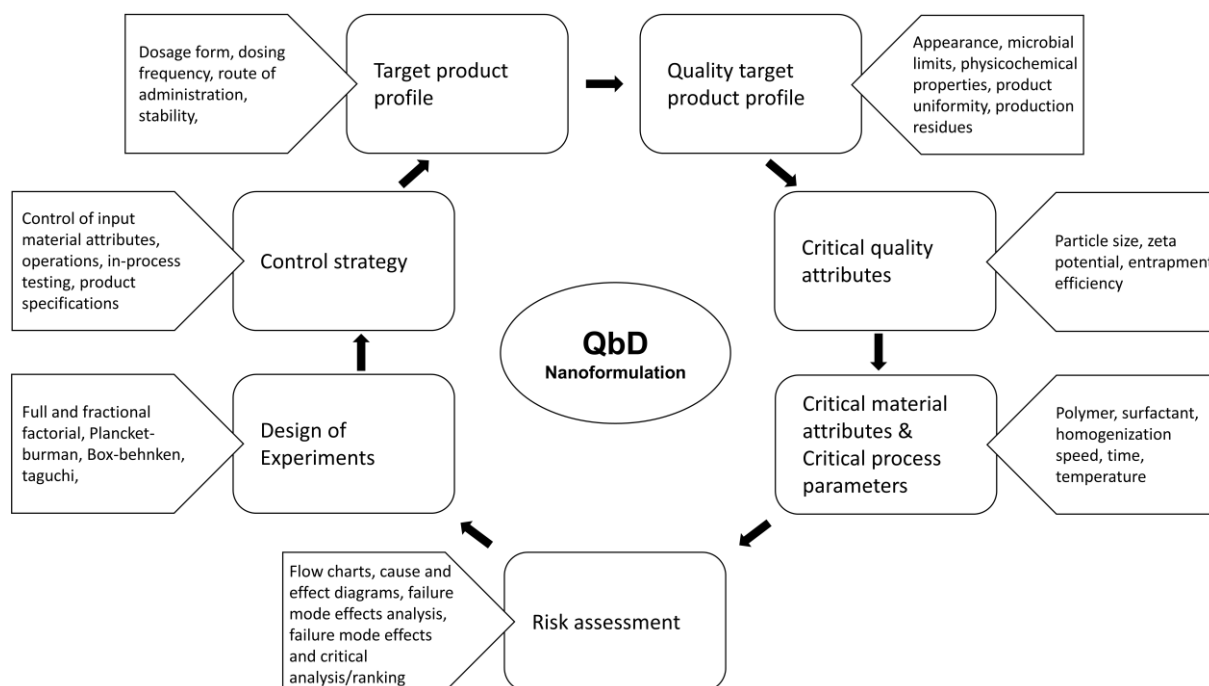


Figure 11: Main elements of the Quality by Design concept in simplified form as applied to a hypothetical nanomedicine¹⁰².

A prospective summary of the ideal product requirements is reflected in the Target Product Profile (TPP), which will be the main project driver. The TPP is a good basis for capturing the design requirements for a new nanoparticle formulation. The TPP usually contains only pharmaceutical and clinical requirements, but can be extended in an industrial environment by additional requirements such as regulatory and commercial/marketing needs. Based on the TPP of a planned formulation and the

patients' needs, a predetermined summary of the essential product characteristics is compiled to ensure the desired quality in terms of product safety and efficacy. For the development of this compilation, called Quality Target Product Profile (QTPP), a comprehensive knowledge of the quality standards of the pharmacopoeias with regard to the planned dosage form/administration form is required. The QTPP can be seen as a link between the biological performance and the physicochemical characteristics of the formulation. Furthermore, the QTPP is used to identify the Critical Quality Attributes (CQA), which can be physical, chemical, biological or microbiological properties or characteristics of a medicinal product, which should be within a defined range to ensure the desired product quality^{100,102}. CQA are then ranked based on their risk or criticality in terms of product efficiency and patient safety. Since CQAs are usually closely related to the materials and processes used, critical material properties (CMA) and critical process parameters (CPP) can be derived through careful risk evaluation or prior knowledge. Both CMA and CPP are able to affect the CQAs.

The risk assessment includes the classification of quality as well as material properties and process parameters into high, medium, and low-risk attributes. The Ishikawa fishbone diagram and failure mode and effects analysis (FMEA) are widely used approaches for risk assessment for the formulation development. These allow root cause identification between the many possible variables influencing the specific quality parameter in the event of the occurrence of deviations in quality¹⁰³. QbD also includes so-called Design of Experiments (DoE), which generally refers to all statistical procedures that are performed before the actual laboratory experiments. These considerations date back to the 1920s, when Ronald Aylmer Fisher introduced basic procedures in the design of experiments in the field of agricultural research, such as repetitions, random sequences, block formation and blending. DoE helps to determine the relationship between the process influencing factors, and the properties of the product. Mathematical models form the basis of this tool. Using computer-aided process design and process simulation, simultaneous evaluation of different factors can be realized in a systematic way with a minimum of experiments. This saves time and costs¹⁰². The result of these efforts, i.e. the application of DoE, risk assessment and process development experiments, is a comprehensive understanding of the influence of material properties and process parameters on product CQAs⁹⁷.

Furthermore, this comprehensive knowledge allows the identification of variables over a wide experimental range, the region of operability (also known as knowledge space)^{98,100} (Figure 12).

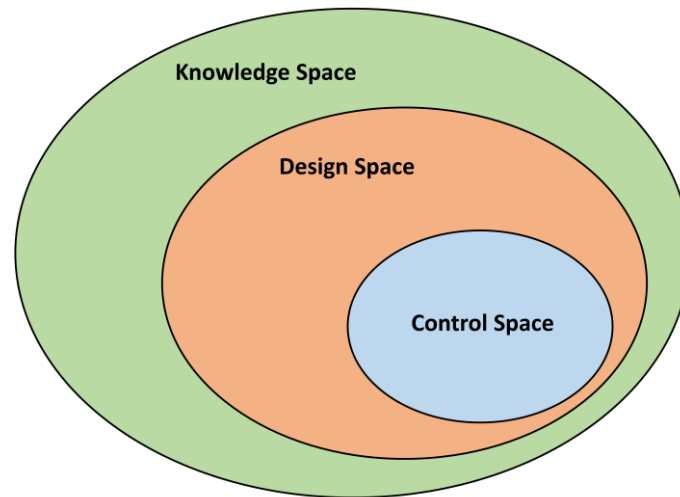


Figure 12: QbD interdependencies. Schematic representation of the relationship between knowledge, design, and control space.

The area within the knowledge space where consistent quality can be achieved is called design space. In the words of the ICH guideline, the design space is the multidimensional combination and interaction of input variables (e.g. material properties) and process parameters that have been proven to serve quality assurance¹⁰⁰. Often within companies, an even narrower and more restricted area is defined within the design space for tighter control of product and process parameters, also known as the control space. In comparison to the design space, however, this control space has no relevance for official regulation. Thus, deviations within the design space are not considered a "change". However, larger deviations from the design space are considered a "change" and would normally initiate a regular change process after approval⁹⁷. As a result, the design space is also regarded as the final achievement of process understanding in the development of new products and processes and therefore belongs to the fundamental paradigms on which the QbD framework is based⁹⁷. This design space has to be continually monitored. Using the acquired process understanding and risk assessment strategy, critical parameters are controlled by a control strategy to stay within the required limits of the design space⁹⁷. ICH Q 10 defines this dynamic element of QbD as follows: "a planned set of controls, derived from current product and process understanding, that ensures process performance

and product quality. The controls can include parameters and attributes related to drug substance and drug product materials and components, facility and equipment operating conditions, in-process controls, finished product specifications and the associated methods and frequency of monitoring and control”¹⁰⁴.

1.4.1 Quality by design inspired approaches in academic research

Academic research in the fields of nanomedicines and nanodiagnostics have much to learn from the QbD approach applied in the pharmaceutical industry. The initial detailed planning and design of experiments would save time and financial resources in an academic environment. Since academic research plays a comparatively large role in the field of novel contrast agent research, and the profit after investment by companies in this area is comparatively low, the field would benefit from an early QbD application in the academic sector^{105,106}. This could take several forms. One useful application of QbD in academic research could be the design of a putative TPP for the novel technology platform. Based on this, an appropriate QTPP can then be devised¹⁰⁶. Even if the resulting QTPPs are not all-encompassing, planning academic studies around the presumed QTPPs has many advantages. They offer a meaningful and structured framework within which the experimental focus can be placed in order to have an early and realistic sense of possible medical applications. Last but not least, QbD-inspired approaches help to produce extraordinarily high-quality samples that would significantly improve preclinical animal studies from an ethical and scientific perspective¹⁰⁶. There are already some pioneers in the field of nanoformulation who have applied such concepts from the beginning^{107–109} and a growing number of documents and methodological standard procedures from organizations (e.g. Nanotechnology Characterization Laboratory) that support this approach and which are available to researchers.

1.4.2 Target product profile for the CPNs investigated in the current study

The CPN suspension is intended to serve the (pre)clinical goal of cancer diagnosis and possibly guided surgery. The application target group are persons of all sexes, all ages and potentially healthy people. The nanodiagnostic is to be administered intravenously. For the in vivo studies in HeLa tumor bearing mice, the dose of 50 µg/mL CP shall be administered only once during the diagnostic procedure and this in a maximum volume of 150 µL. The nanosuspension in question should be sterile and should not cause any

adverse side effects. The effectiveness of the diagnostic should be given with an SBR greater than 1.1¹¹⁰.

Based on this TPP, a QTPP was compiled (Table 1) to ensure the safety and efficacy of the nanodiagnostic in the in vivo study. The resulting quality characteristics of the formulations are shown schematically in Figure 13 in a hypothetical application environment. Tables in Publications II and III list critical quality attributes (CQA) with a traffic light system, according to which they are ranked with regard to the risk potential for efficacy and safety of the formulations. These tables also include product specifications and acceptance criteria ranges.

Table 1: General QTPP for CPN

Quality product profile	Target
Appearance	no visible matter
Microbial limits	BET, CFU in defined range
Physicochemical properties	Particle size, PDI suitable for in vivo application Colloidal stable in physiologic environment pH and tonicity suitable for in vivo application
Product uniformity	Consistently high yields and fluorophore content
Production residues	Solvent residues in acceptable range

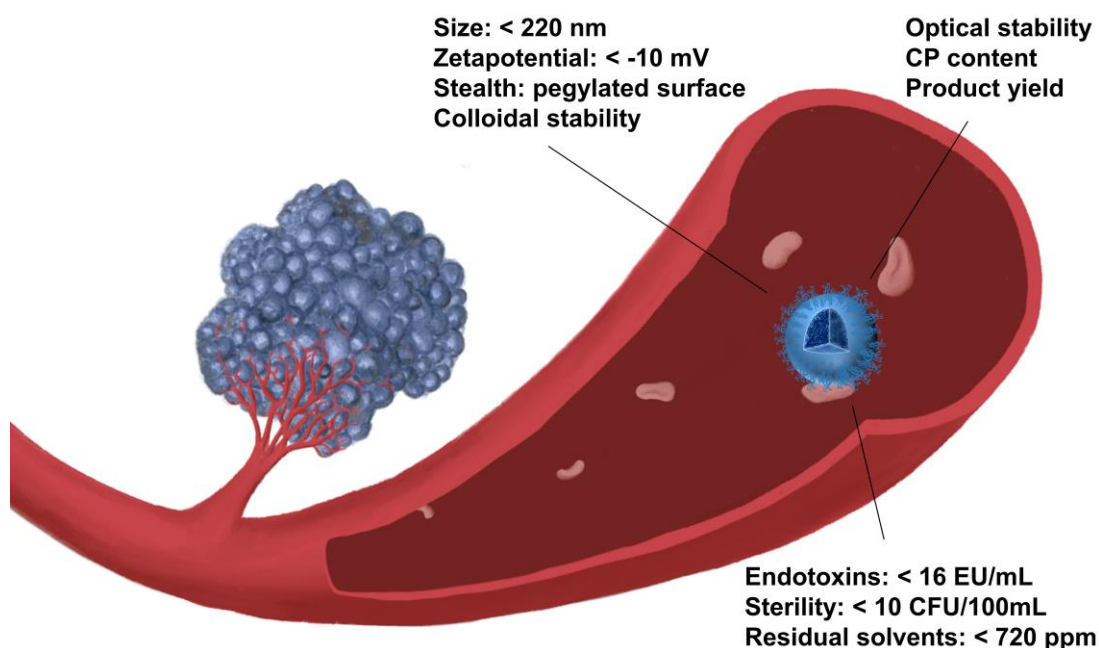


Figure 13: Blood vessel with vascularized tumor and administered CPN. Labeling indicates critical quality properties of a CPN for intravenous use.

1.5 CPN formulation strategies

The lipophilic CPs of this study require processing into an aqueous nanoparticle suspension using suitable methods such as nanoprecipitation^{14,111,112} to enable a potential in vivo application¹¹³. CPs can be easily processed into nanoparticles and are very attractive materials in this form due to the enhancement of their properties^{63,114–116}. CPNs are well suited for biomedical applications due to their high photostability, high quantum yields (quotient of emitted photons in relation to absorbed ones), high extinction coefficients and negligible toxicity^{90,117}. The following possible biomedical applications should be briefly mentioned in particular: Fluorescence and photoacoustic imaging, long-term cell imaging¹¹², image-guided drug and biomolecule delivery, stimuli-responsive NP for controlled cargo release^{118–120}, light induced sensitizers for photodynamic therapy, photothermal therapy and combinations¹²¹ of these applications, so-called multiplexed probes¹²¹.

The encapsulation of CPs into a matrix or the use of a coating material to form NPs are two methods of CP incorporation into nanoparticles frequently reported in the

literature¹¹⁴. These processing strategies aim to control surface properties and ensure colloidal stability in physiological media. Furthermore, surface modification can enable active targeting strategies whereby antibodies or substrates from overexpressed receptors of tumors are conjugated on the nanoparticle surface which leads to an increased accumulation in the target tissue and thus to an increased contrast^{14,122–125}. In addition to polymers, lipids, surfactants and proteins have already been successfully exploited for CPN production purposes¹⁴.

In the present study two different CPN architectures were investigated (Figure 14): 1) CP embedded within another matrix, such as a polymer or inorganic material and 2) core-shell nanoparticles with CP as a core coated with a phospholipid or surfactant shell^{14,120,121}. To achieve these different architectures, CPNs were prepared using a modified nanoprecipitation method in the presence of different pharmaceutical excipients. In Formulations I and II, the CPs were embedded within self-assembling poly(ethylene glycol) methyl ether block poly(lactide-co-glycolide) or PEG-PLGA polymer micelles, and are referred to as matrix type CPNs. To understand the impact of the matrix polymer, PEG-PLGA, on the CPN attributes two grades of PEG-PLGA, PEG_{2kDa}-PLGA_{4kDa} and PEG_{5kDa}-PLGA_{55kDa}, were chosen for this study. These two PEG-PLGA block copolymers differed not only in molecular weight of PEG and PLGA but also in the composition of the PLGA. The glycolic acid:lactic acid ratio was 34:66 for PEG_{2kDa}-PLGA_{4kDa} and 50:50 for PEG_{5kDa}-PLGA_{55kDa}. In the Formulation III, the CP precipitated out of the solvent to form the nanoparticle core, which was then coated in situ by the phospholipid surfactant, 1,2-dipalmitoyl-sn-glycero-3-phosphoethanolamine-N-[methoxy(polyethylene glycol)-2000] (PEG_{2kDa}-DPPE). It was hypothesized that CPNs produced in this manner would adopt a core-shell structure with the core comprised nearly exclusively from the CP, which is then coated with the phospholipid surfactant. For this reason, we refer to this formulation as a core-shell system (Figure 14).

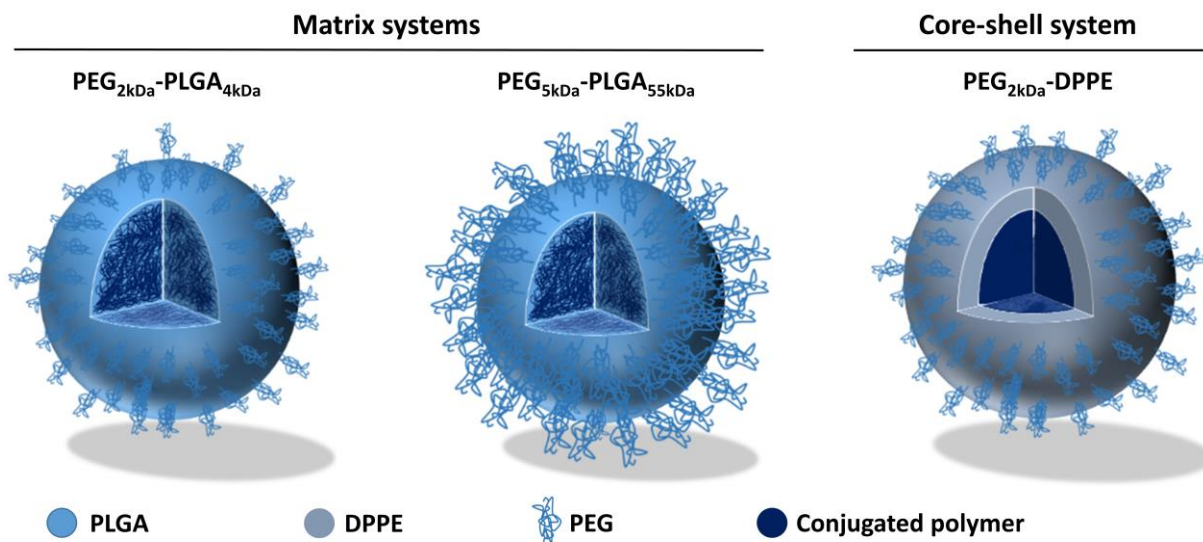


Figure 14: Different CPN architectures, matrix systems and core-shell systems used.

One of the postulated differences between the core-shell type architecture, which relies on adsorption of pegylated surfactants to the lyophobic CP core, and the matrix-type architecture is the possibility of surfactant displacement by serum proteins following intravenous administration^{126,127} and the formation of a protein corona¹²⁸. While matrix-type CPN often feature pegylated surfaces, the PEG groups are in general covalently attached to the matrix core, making displacement of the PEG surface coating less likely. This concept was recently published, demonstrating that core-shell PLGA nanoparticles, which are coated with the amphiphilic polymer polyvinyl alcohol, show a much higher serum protein surface adsorption than PEG-PLGA matrix systems, where the PEG groups are covalently attached to the PLGA matrix. The difference in protein corona formation as a function of nanoparticle architecture is postulated to have an effect on nanoparticle biodistribution following intravenous administration¹²⁹. It was hypothesized that the core-shell type formulation (Formulation III: PEG_{2kDa}-DPPE CPNs) would show a higher opsonization (i.e., protein corona formation) and therefore show a different biodistribution profile compared to PEG-PLGA CPN systems (Formulations I and II).

The amphiphilic, self-assembling di-block copolymer PEG-PLGA is a popular matrix material for nanoparticles¹³⁰. The first targeted nanomaterial to be clinically tested on humans was a PEG-PLGA-based nanoformulation containing docetaxel for anti-cancer therapy¹³¹. Due to its amphiphilic character, PEG-PLGA has the ability to assemble itself into nanoparticles in water¹³². PLGA is approved by the FDA and is

biodegradable¹³³. The bound PEG aligns itself to the hydrophilic phase during NP production and thereby has a great influence on the nature of the NP surface. The pegylated surface increases the systematic circulation time via the resulting stealth effect by binding fewer and more selectively proteins, which in turn reduces unspecific cell uptake and evades clearance by the immune system^{134,135}. In addition to pegylation, the pharmacokinetics of NPs are also influenced by factors such as particle size distribution, shape and material composition¹³⁶.

For a desired in vivo application, nanoparticles have been described over a wide range in the nano-size range, but the properties in the 5-250 nm diameter range are particularly useful¹³⁷, as this results in physiological advantages and the resulting nanoparticle suspension (< 220 nm) can be sterile filtered without major losses in product yield.

Nanoparticle formulations designed for systematic administration are immediately exposed to a complex environment when they are administered into the systematic circulation¹³⁴. Physiological biomolecules interact with the surface of the nanoparticles and are deposited on it, thus forming a protein corona¹³⁸. The resulting opsonization of the nanoparticles, i.e. the labelling with antibodies and factors of the complement system, leads to rapid recognition by phagocytic immune cells, which take up and eliminate the nanoparticles thus identified¹³⁹. In this context the previously described effects of a pegylated NP surface lead to a lower immunogenicity and a slower degradation rate by metabolic enzymes and thus to a more favorable pharmacokinetics after systemic application^{129,140}. The NP clearance from the systemic circulation is based, among other things, on morphological characteristics of the endothelia of the blood capillaries, which are classified as continuous, fenestrated or discontinuous; accordingly, it is size-dependent¹³⁷. Which type a capillary belongs to depends on the density of its structure, and the structural density decreases from continuous to fenestrated to discontinuous capillaries. The capillary type is also organ-specific and morphologically variable between mammalian species. Capillaries of the skin, heart, lung and skeletal muscles, have the most common type of capillary, i.e. continuous capillaries. The endothelia of the kidneys exhibit fenestrated capillaries with pores of between 20 and 80 nm. Discontinuous capillaries with gaps between 50-180 nm are predominant in the liver and can be up to 5 µm in the spleen. Thus NP are eliminated

by the kidney depending on their size ($< 5 \text{ nm}$)¹⁴¹ or accumulate in the liver and spleen via diffusion through the gaps of discontinuous capillaries^{20,142}.

CPN architecture and attributes not only influence the pharmacokinetic behavior of these nanodiagnostics, but can often influence their optical performance. It has often been observed that the spatial confinement of the CP resulting from encapsulation within in various nanoparticle structures can dramatically affect the optical properties¹¹⁴. For example, blue-shifted and broadened absorption spectra indicate a general decrease in the conjugation length of polymers due to bending, torsion and kinking. In contrast, the frequently observed redshift of the emission maximum points to the formation of aggregates between the individual chains rather than to self-aggregation by coiling^{64,143}. These observations are rooted in the altered electron mobility across the spatially confined conjugated backbone of polymers^{76,89}. Therefore, it can be concluded that a thorough and systematic investigation of critical processing parameters is needed to adequately characterize CPN material, quality, safety and performance attributes.

2 Aim of the project

The objective of this project was to investigate three novel CPN systems for their performance in fluorescence and photoacoustic diagnostic applications using both in vitro and in vivo methodologies. Where possible, a QbD-inspired approach was implemented in order to produce systems that conformed with pharmaceutical quality standards for intravenously administered formulations. The primary study question addressed in this work was whether formulation composition, e.g. the PEG-PLGA matrix material (Formulations I and II) or CPN stabilization strategy (Formulation III) significantly influenced physicochemical characteristics, optical and photoacoustic properties, biocompatibility, in vivo biodistribution and imaging performance.

The first publication describes the physicochemical properties, biocompatibility and fluorescence/photoacoustic performance of CPNs with different low molecular weight PEG-PLGA polymers as matrix. In this study the influence of the different PEG-PLGA matrices on physicochemical properties, biocompatibility and in vitro imaging

performance was of interest. It was hypothesized that an increase in PLGA molecular weight in the diblock copolymer could lead to an increase in nanoparticle size but could also have a beneficial effect on the optical properties of PCPDTBT as the nanoparticle core of Formulation II would be more hydrophobic compared to Formulation I due to the increased PLGA molecular weight. The hydrophobic environment could reduce self-aggregation and coiling of the CP in the nanoparticle core thereby promoting electron mobility across the CP backbone^{64,143}. The hypothesis that the embedded PCPDTBT would not affect the biocompatibility of the nanoparticles was also the subject of this investigation. My practical contribution to this study included the production of the different CPN formulations, physicochemical characterization (size, zeta potential, colloidal stability), cell viability assessment (MTT assay), optical characterization (spectra and photoluminescence quantum yield (PLQY)) and evaluation of fluorescence and photoacoustic imaging performance.

The second publication utilizes the knowledge gained in the first study to determine whether the differences between PEG-PLGA formulations I and II observed during the in vitro investigation were also apparent in an in vivo model. In this study, both matrix CPNs containing PCPDTBT (Formulations I and II) were compared with core-shell CPNs also containing PCPDTBT (Formulation III). It was hypothesized that the core-shell CPNs stabilized with PEG_{2kDa}-DPPE (Formulation III) would show a higher surface protein binding via surfactant displacement compared to PEG-PLGA CPNs (Formulations I and II) and therefore a faster liver accumulation in vivo.

The third publication describes the in vivo optical performance of a novel 100% borylated PF8-BT, P4, which was previously investigated for optical properties in vitro⁹³. The major study question addressed here was whether the outstanding in vitro optical properties of P4 CPN could be observed in an in vivo mouse xenograft model. Further, it was assessed whether CPNs are superior to the FDA-approved NIR dye, ICG, in terms of in vitro optical performance. It was hypothesized that the two π -conjugated polymers, PCPDTBT and P4, would show a higher resistance to photobleaching than ICG and that P4 CPNs would be superior to PCPDTBT in optical in vivo performance.

In Chapter 4, the results of the work presented in this thesis are discussed in the context of the current state-of-the-art of optical and PA contrast agent development.

Short term and long term perspectives on the development of CPNs as novel contrast agents are provided.

3 Cumulative part

3.1 general information on scientific journals

Table 2: General information on scientific journals.

Title	Journal of Material Science B	Applied Materials and Interfaces	Advanced Healthcare Materials
Impact Factor	5.344 (2019)	8.758 (2019)	7.367 (2020)
5-Year Impact	5.022	7.837	5.941
Publisher	Royal Society of Chemistry	American Chemical Society	Wiley-VCH

3.2 Itemization of own contribution

Table 3: Specification of the percentage of own contribution to the publications. The own contribution is made up as follows.

A: own contribution to the planning, the execution, the analysis of the experiments and the preparation of the corresponding illustrations.

B: own contribution to the preparation of the manuscript.

Publication I	<p>Low molecular weight PEG-PLGA polymers provide a superior matrix for conjugated polymer nanoparticles in terms of physicochemical properties, biocompatibility and optical/photoacoustic performance</p> <p><i>Thais Fedatto Abelha, Paul Robert Neumann, Joost Holthof, Cécile A. Dreiss, Cameron Alexander, Mark Green, Lea Ann Dailey</i></p> <p>J. Mater. Chem. B, 2019,7, 5115-5124</p> <p>A: 50% B:50%</p>
Publication II	<p>Different PEG-PLGA matrices influence in vivo optical / photoacoustic imaging performance and biodistribution of NIR-emitting π-conjugated polymer contrast agents</p> <p><i>Paul Robert Neumann, Frank Erdmann, Joost Holthof, Gabriela Hädrich, Mark Green, Jianghong Rao, Lea Ann Dailey</i></p> <p>Adv. Healthcare Mater. 2020, 2001089, 1-13</p> <p>A: 85% B:80%</p>
Publication III	<p>In Vivo Optical Performance of a New Class of Near-Infrared-Emitting Conjugated Polymers: Borylated PF8-BT</p> <p><i>Paul Robert Neumann, Daniel L. Crossley, Michael Turner, Michael Ingleson, Mark Green, Jianghong Rao, and Lea Ann Dailey</i></p> <p>ACS Appl. Mater. Interfaces 2019, 11, 50, 46525–46535</p> <p>A: 75% B:75%</p>

The following section contains three publications, which were published as research articles in international journals following the peer-review procedure. These articles constitute the basis of my work and summarize the experimental results. The articles are closely related, with the first article focusing on the investigation of the influence of the molecular weight of PEG and PLGA of PEG-PLGA diblock copolymers as nanoparticle matrix for the conjugated polymer PCPDTBT on basic nanoparticle properties (particle size; zeta potential) and furthermore on cell viability and optical/photoacoustic properties in vitro.

In the second publication, PCPDTBT was again embedded in PEG-PLGA matrices, additionally a further nanoparticle formulation that coated the conjugated polymer with a phospholipid was included in the study. Again, the Quality by Design inspired approach for nanoparticle characterization was applied to guarantee safe formulations in the following in vivo investigations of the performance of the formulations using fluorescence and photoacoustic imaging. The observed biodistribution prompted further experiments regarding the protein corona that forms around the nanoparticles in the physiological environment.

In addition to PCPDTBT, the third publication highlights another conjugated polymer, a boronated F8BT (P4), synthesized by cooperation partners from the University of Manchester. These and the small molecule dye ICG were embedded in one of the PEG-PLGA matrices for nanoparticle production, which were already used in the first and second publication. The resulting nanoparticle formulations were thoroughly characterized in-situ and in vitro prior to in vivo fluorescence application in a xenograft mouse model.

3.3 Publication I

Low molecular weight PEG-PLGA polymers provide a superior matrix for conjugated polymer nanoparticles in terms of physicochemical properties, biocompatibility and optical/photoacoustic performance

Link publication:

<https://pubs.rsc.org/en/content/articlelanding/2019/tb/c9tb00937j> - !divAbstract

Link supporting information:

<http://www.rsc.org/suppdata/c9/tb/c9tb00937j/c9tb00937j1.pdf>

Cite:

J. Mater. Chem. B, 2019,7, 5115-5124

3.4 Publication II

Different PEG-PLGA matrices influence in vivo optical/photoacoustic imaging performance and biodistribution of NIR-emitting π -conjugated polymer contrast agents

Link publication: <https://onlinelibrary.wiley.com/doi/full/10.1002/adhm.202001089>

Link supporting information:

<https://onlinelibrary.wiley.com/action/downloadSupplement?doi=10.1002%2Fadhm.202001089&file=adhm202001089-sup-0001-SuppMat.pdf>

Cite: *Adv. Healthc. Mater.* 2020, 2001089, 1–13

3.5 Publication III

In Vivo Optical Performance of a New Class of Near-Infrared-Emitting Conjugated Polymers: Borylated PF8-BT

Link publication:

<https://pubs.acs.org/doi/abs/10.1021/acsami.9b17022>

Link supporting information:

https://pubs.acs.org/doi/suppl/10.1021/acsami.9b17022/suppl_file/am9b17022_si_001.pdf

Cite:

ACS Appl. Mater. Interfaces 2019, 11, 50, 46525–46535

4 General discussion

The intent of this body of work was to make a contribution to the further development of CP-based contrast agents. Optical imaging for diagnostic purposes is mainly held back by photon-limited interference with the tissues under examination. Despite decades of research in this field, optical imaging methods are still relatively rare in the clinic (Figure 1). It is widely believed that with the development of better exogeneous contrast agents, optical imaging would increasingly become standard clinical practice. Small molecule dyes such as fluorescein, methylene blue, ICG, as well as the precursor dye, 5-aminolevulinic acid, have FDA approval and are in clinical use. According to a recent publication, the pipeline is currently filled with 39 new contrast agents for fluorescence image-guided surgery (FGS). As novel contrast agents are considered new drugs by the FDA, they also have to go through lengthy and expensive approval processes before they can ultimately be used clinically⁵³. Although some of these dyes have been in clinical use for a long time for diagnostic purposes such as angiography, visualization of cancer cells and organs, they also have disadvantages such as photobleaching and small Stokes shifts. Although these dyes can also be functionalized and processed into nanoparticles so that they can actively mark their target, thereby overcoming disadvantages such as the extremely fast clearance from the site of interest, optical disadvantages remain¹⁴⁴. CPs, however, offer the possibility of overcoming the optical disadvantages of traditional molecular dyes and are currently in the focus of intensive research. The following sections highlight how the research studies presented here have contributed to our general knowledge and development of CP-based nanodiagnostics for optical and PA imaging applications.

4.1 QbD inspired CPN research

For a potential in vivo application, CPN formulations must meet high quality requirements. Testing CPN formulations for size, surface charge and cell viability is standard practice for scientists in this discipline. Less common are tests for haemocompatibility, such as those performed in publication I. In addition, publications II and III incorporated a QbD inspired approach to pharmaceutical assessment of the

CPNs and as a consequence reported a wider range of critical quality attributes, such as product yield, loss on sterile filtration, colloidal stability, content uniformity, residual solvent levels, sterility and endotoxins. The assessment of many of these parameters is currently very rare in the field of CPN research, which is dominated by researchers without a pharmaceutical science and drug development background. Thus, one of the most important contributions to the field of CPNs and nanodiagnostic research achieved by this work is the demonstration of how pharmaceutical quality parameters can and should be incorporated into nanodiagnostic studies, even at a very early research stage, as this will play an important role in the translational of novel contrast agents into the clinic.

4.2 The impact of nanoparticle architecture and composition on CP optical properties

As mentioned in Section 1.5, the optical properties of fully dissolved CP in solution differ considerably from that of CP incorporated into CPN. This is attributed to the changed conformation of the conjugated polymers within the NP, whereby the conjugation length is reduced and the individual polymer chains are more tightly packed than in the dissolved state, which results in an altered electron flow across the polymer backbone^{70,145}. Two optical characteristics, the maximal absorption/emission wavelength and PLQY are typically used to assess the effects of CPN architecture and composition on CP optical behavior. For fluorescence imaging applications, I was initially working under the hypothesis that both a shift in the absorption and emission spectra towards the tissue transparency window, as well as a high PLQY would be favorable for in vivo fluorescence imaging. In contrast, PAI contrast agents should have a high absorption in the tissue transparency window and a low PLQY.

Figure 15 shows the maximum emission peaks (B, D) and PLQY (A, C) of CPN formulations presented in this thesis compared to a selection of comparable formulations published in the literature^{90,93,146–148}. The formulation of the nanoparticles has a great influence on the conformation of the CP processed in them, which in turn affects the optoelectronic properties of the CP to a particular extent, as already mentioned in 1.5. Thus, it was demonstrated that a silica as a shell material favored the fluorescence performance of PCPDTBT. The authors suggested that the non-polar

environment created by silica for the CP was crucial for this enhanced performance¹⁴⁶. Crossley et al. also showed higher PLQY with silica CPN compared to PEG-PLGA CPN⁹³. The core shell NP architecture of CP and 1,2-dioctanoyl-sn-glycero-3-phosphocholine (DOPC) or 1,2-dioctanoyl-sn-glycero-3-phosphoethanolamine (DOPE) gave PLQY values comparable to solutions of CP in nonpolar solvent, which is why the authors assumed the absence of water molecules in the NP⁹⁰. They also showed that the CP in the CPN is in short-range association, but the WAX profile showed no well-developed diffraction peaks, which contradicts a completely crystalline core. By processing CPs into a liquid core of midchain triglyceride (MCT), lipid nanocapsules (LNC) were formed, which resulted in comparatively high PLQY values comparable to the CPs in silica shells¹⁴⁸. It was also observed that both the LNC and the silica CPN showed the lowest red shift in the emission spectrum (Figure 15 B). A more coiled conformation and the presence of molecular aggregates of the polymer leading to a more efficient energy transfer among the backbones is reported to result in red-shifts in the emission spectra. These shifts are typically accompanied by a substantial aggregation-induced quenching (i.e. decrease in the quantum yield). Generally, a high PLQY is assumed to result in good fluorescence performance, as this suggests that the absorbed energy is primarily released via fluorescence, while a low PLQY is assumed to result in non-radiative energy dissipation, for example via vibrational relaxation, which hypothetically will result in a PA signal¹⁴⁷.

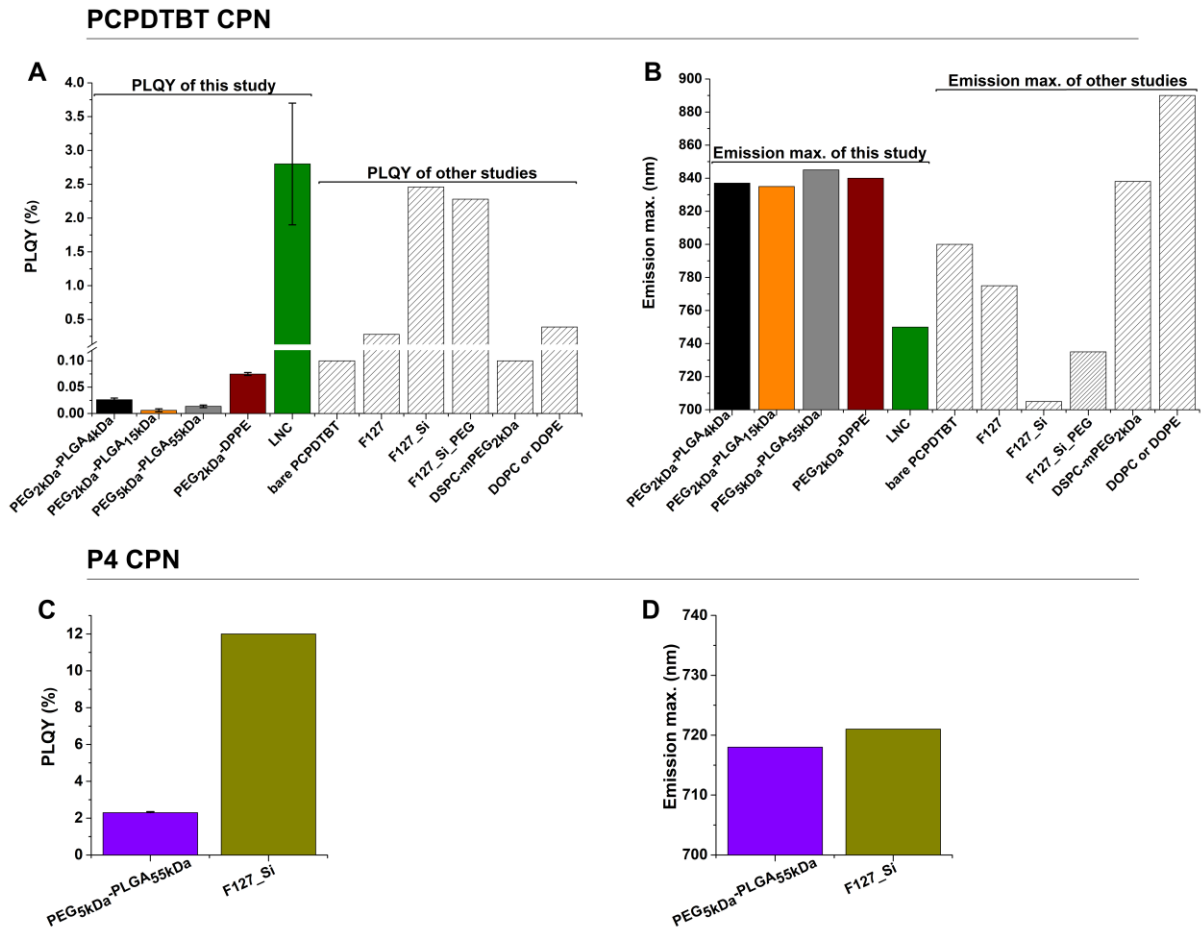


Figure 15: PLQY and maximum emission peaks of PCPDTBT CPN of this study and a selective representation from other recent studies (A; B) and of CPNs of the novel CP P4 (C; D). Colored bars with error bars originate from our studies^{93,95,148,149}, they represent the mean \pm standard deviation of (n = 3) independently produced batches per formulation. White bars with diagonal stripes originate from current literature^{90,146,147}.

4.3 PLQY is not predictive of fluorescence imaging performance in a phantom mouse and in vivo mouse model

The hypothesis that higher PLQY values also perform better in fluorescence imaging procedures was only true in isolated cases and therefore cannot be confirmed in general. In our study, when comparing PEG_{2kDa}-PLGA_{4kDa}, PEG_{2kDa}-PLGA_{15kDa} and PEG_{5kDa}-PLGA_{55kDa} as matrix materials of PCPDTBT, the in vitro SBRs followed the PLQYs, although there were only marginal differences in PLQY and also the SBRs showed very similar values¹⁵⁰. In one of our other publications, we were able to measure a 3-4x higher PLQY for a PEG_{2kDa}-DPPE CPN compared to the PEG-PLGA matrix CPNs, but nevertheless the DPPE CPNs showed a 30% lower SBR in IVIS fluorescence imaging¹⁴⁹.

Also in vivo, PEG_{2kDa}-DPPE CPN did not show performance advantages in fluorescence imaging corresponding to the higher PLQY. When comparing the novel CP P4 against PCPDTBT CPN (publication 3)¹⁵¹, P4 showed a significantly higher PLQY and also higher SBRs in fluorescence imaging in vitro, however, in vivo the tumor periphery ratio of the two CPN systems is almost identical due to the higher fluorescence signal of P4 in the periphery. Active targeting could improve the in vivo performance of the P4 CPNs in this regard. The LNCs loaded with PCPDTBT showed PLQY values comparable to P4 PEG-PLGA CPN, which also showed similarly high SBRs in in vitro fluorescence imaging¹⁴⁸.

Zhu et al. showed a clear correlation between PCPDTBT CPN formulation and optical properties¹⁴⁶. Processing in a silica shell increased PLQY values compared to bare PCPDTBT CP and CPN processed in poloxamer F127. In this study, higher PLQY also resulted in better fluorescence imaging performance. In vivo, silica CPNs showed bright signals, however, despite slightly lower PLQY, the pegylated variant outperformed the unpegylated silica CPN due to significantly better biodistribution.

Pu et al. compared PCPDTBT with various DPP-based CPs, which they processed with lipids (dipalmitoylphosphatidylcholine (DPPC), 1,2-distearoyl-sn-glycero-3-phosphoethanolamine-N-[methoxy(polyethylene glycol)-350] (DSPE-mPEG350), and DSPE-mPEG2000) to form CPN¹⁴⁷. The CPN showed low PLQY values that differed by a factor of 10-100. CPNs with higher PLQY also showed higher signals in vitro fluorescence imaging.

Although the latter two studies^{146,147} suggest predictability of PLQY values and in vitro fluorescence imaging performance, it should be noted that both studies tested in vitro performance without a phantom mouse. This has a decisive influence on the in vitro performance due to the simulation of light scattering and absorption of a living mouse.

4.4 The impact of CPN architecture on PA imaging performance in a phantom and in vivo mouse model

PCPDTBT CPN formulations have been tested not only for their fluorescence but also for their photoacoustic imaging performance. During the investigations it was found that the different CPN architectures and compositions have an influence on the PA

imaging performance. For example, we observed that the PA signal amplitude of PEG-PLGA CPNs was unstable over time and decreased with prolonged laser irradiation (Figure 16 B). In contrast the core-shell PEG_{2kDa}-DPPE CPNs showed a lower, but steady signal amplitude over the entire study period (Figure 16 C), which was comparable to results reported by Pu et al. using a similar CPN architecture⁶².

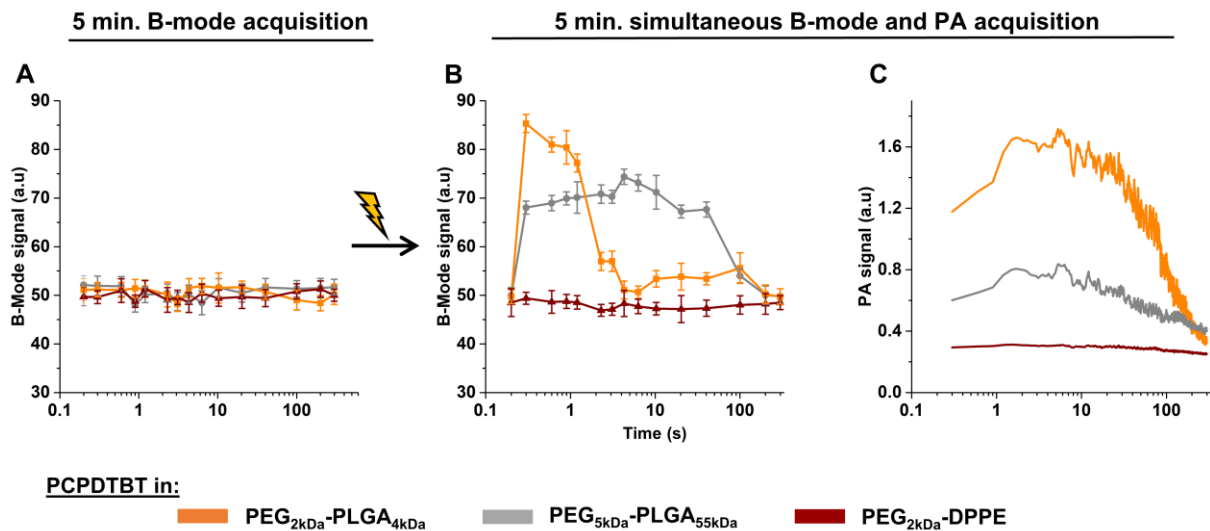


Figure 16: A) Time-dependent B-mode signal of the CPNs at selected measurement times over the measurement period of 5 min, while only the ultrasound probe is switched on. B) Time-dependent B-mode signal at selected measurement times and C) PA signal of the CPNs over the measurement period of 5 min, while both the ultrasound probe and the laser are switched on. Data in panels (A) and (B) represent the mean \pm standard deviation of ($n = 3$) independently produced batches per formulation¹⁴⁹.

Such observations led to the question of why different CPN architectures show different PA signals despite very similar optical properties. The lower PLQY of PEG-PLGA CPNs indicates a preference for non-radiative decay, resulting in higher PA amplitudes compared to PEG_{2kDa}-DPPE. However, the PEG_{2kDa}-PLGA_{4kDa} CPNs show a higher PA amplitude than the PEG_{5kDa}-PLGA_{55kDa} despite a larger PLQY. PLQY and spectra alone cannot predict in vitro PA performance. This was also confirmed by another study by Modicano et al. in which PCPDTBT was processed with MCT as LNCs. The LNCs showed slightly lower PAI performance compared to the PEG-PLGA and PEG-DPPE CPNs despite significantly higher PLQY¹⁴⁸.

The LAZR-X used for PA imaging shows the PA signal as well as the B-mode image i.e., the 2D grayscale image in sonography due to the parallel ultrasound imaging. Especially at the beginning of the measurement, a B-mode signal could be observed with the PEG-PLGA CPN, but not with the PEG_{2kDa}-DPPE formulation (Figure 16 B). It

turned out that the ultrasound alone could not increase the contrast (Figure 16 A). The simultaneous contrast increase in B-mode and PA signal was only realized by switching on the laser.

Pu et al. concluded that the different lipids they used as CPN shell material had a negligible influence on the PA imaging performance¹⁴⁷. They further concluded that the PA intensities of CPNs are mainly determined by the molecular structures of CPs. In their study, they also showed that CPNs with lower PLQY values have better PAI performance in vitro. It is possible that a general prediction of the in vitro PAI performance and distinct differences of the PA signals of CPNs is only possible from larger differences of the PLQY values (10-100 fold) of the CPNs under investigation.

4.5 PA and B-mode contrast enhancement mechanisms

The strong contrast increase initiated by the laser was, as already mentioned, only observed in the PEG-PLGA formulations. It can be assumed that the optically triggered dual contrast enhancement is caused by gas bubbles created by vaporization⁵². It has already been described that the generated gas bubbles increase both the ultrasonic and the PA contrast agent⁵². Over the experimental period of 5 minutes, the B-Mode contrast of the PEG-PLGA CPN returns to its initial value (Figure 16 B). Over the same period of time, the PA signal generated by PEG-PLGA formulations converges to that of PEG_{2kDa}-DPPE (Figure 16 C).

Possible differences in the thermal conductivity and the heat capacity of the matrix material could confine the heat generated by the CP to a different extent in the PEG-PLGA CPN. These hypothetical differences in thermal confinement could lead to different temperatures in the CPN. These differences in turn could influence the expansion and relaxation amplitudes and thus the PA signal^{52,152}. The generation of nanobubbles can also be influenced by these properties of the nanoparticle material. A better insulating envelope material hypothetically leads to higher core temperatures in the NP and is therefore more likely to cause a liquid to gas transition⁵².

5 Outlook and perspectives

5.1 Further developments of CPN technology

Parallel to our work there were novel developments in the field of CPNs. Recent review articles provide an excellent overview of the different types of CPN chemistries and their preclinical safety assessment as well as the wide range of applications from optical imaging including fluorescence, photoacoustic, multimodal and activatable imaging techniques to imaging-guided phototherapy and combination therapy, light-triggered drug delivery and gene regulation^{14,153}. Furthermore, possibilities for active targeting of CPN also in combination with therapeutic applications have already been described^{60,154}.

Two examples were especially innovative. In one study, CPs were linked to proenzymes or enzymes and their activity was specifically activated by NIR irradiation in the tumor to enable theranostic approaches like photodynamic therapy (PDT) and photothermal therapy (PTT). PDT uses the CP properties of imaging, good light-harvesting and energy transfer to a photosensitizer to generate therapeutic ROS. PTT, which is possible with nanocarriers of CPs, makes use of their ability to generate hyperthermia locally after light excitation. PDT and PTT can specifically kill tumor cells or bacteria¹²². Although active targeting leads to higher accumulation in the target tissue, there are still peripheral, non-specific depositions, so research is currently also conducted on protherapeutic CPNs, which can only be activated by the simultaneous presence of biomarkers overexpressed in the tumor microenvironment and an external stimulus such as NIR light¹⁵⁵.

5.1.1 PCPDTBT-ribonuclease A conjugates for PDT and PTT

Recently the synthesis of an organic semiconducting pro-nanoenzyme (OSPE) was reported for cancer therapy and tumor monitoring. PCPDTBT based conjugated polymer was linked to an inactive proenzyme via a singular oxygen cleavable linker. The proenzyme is a cytotoxic ribonuclease A, which is inactivated by a phenylboronic acid pinacol group. During the in vivo application of this formulation, NIR irradiation of the conjugated polymer generates singular oxygen, which enables PDT and cleaves the inactive proenzyme. The biochemical mediator H₂O₂, which is present in the tumor microenvironment, reactivates the proenzyme. The enzymatic activity thus restored

causes intracellular RNA degradation and thus cell death, which inhibits tumor growth and stops lung metastasis¹⁵⁶.

5.1.2 PCPDTBT-Bromelain conjugates for PTT

In another study, PCPDTBT was modified with carboxyl-PEG groups and the resulting amphiphilic molecules were further covalently linked to bromelain. By irradiating the nanoparticle formulation after intravenous administration, a temperature increase was achieved which activated the collagen-degrading enzyme bromelain. It was shown that the extracellular tumor matrix can be degraded and the passive accumulation of nanoparticles can be increased. The laser power was increased 6h after i.v application to perform PTT on the tumour. This approach suppressed 4T1 tumour growth in mice over the experimental period of 16 days¹⁵⁷.

These described results of the current basic research of conjugated polymer nanoparticles provided fundamentally new approaches for tumor monitoring and therapy. Nevertheless, these studies lack the implementation of quality by design approaches. Although the feasibility studies are extremely valuable, rigorous formulation quality requirements implemented from the very beginning with regard to their planned administration route would strongly support further development. Moreover, such a rational experimental approach in early research and development has the potential to bridge the large gap between material science, preclinical experiments and clinical reality and thus accelerate the translation into clinical application.

5.2 Barriers to clinical translation and future work

The absence of CP degradation and elimination has so far prevented its safe in vivo application. This hinders the transfer of CPN to the clinic for use as high performing fluorescent and photoacoustic contrast agents for medical imaging applications. The particles of this study are only partially biodegradable, due to their biodegradable PEG-PLGA or PEG-DPPE structure. In contrast, the CP is hypothesized to persist in the liver and spleen after accumulation. CPs are generally non-degradable due to their

inert and carbon-based π -conjugated architecture¹⁵⁸. It could be that they are excreted very slowly through the feces due to their very lipophilic nature. At this time no statements can be made from our work about their elimination, because the animal excretions were only examined visually during our in vivo imaging study, but not with fluorescence measurement methods. The clearance of CPNs requires investigation for potential in vivo use and transfer into clinical application, therefore these studies should be the subject of further experiments. For this purpose, longer experimental periods should be considered and valid quantification methods must be developed.

However, there are approaches to design biodegradability into the CP structure. For example, biodegradable benzobisthiadiazoles have been synthesized and studied as contrast agents for photoacoustic brain imaging. To examine biodegradation rate and elimination, both the excretions (urine/feces) and the blood of the experimental mice were examined for fluorescent degradation products over a period of two weeks. The benzobisthiadiazoles (BBT) based CPs were embedded within a biodegradable PEG-PLGA matrix. Interestingly, the CPs themselves exhibited a weak fluorescence, whereas the degradation process produced fragments (≈ 1 nm) with a substantially stronger fluorescence. Biodegradation of the BBT polymers was shown to occur in the presence of biologically relevant peroxidase and lipase enzymes. As a result of the enzymatic degradation, the fragments could be continuously eliminated by hepatobiliary and renal excretions¹¹³.

Further recently published concepts for the biodegradability of CPNs were inspired by nature¹¹¹. In these studies, the molecules responsible for bioluminescence of different organisms were looked at. These natural substances such as coelenterazine, vargulin and green fluorescent protein all contain imidazole units in the conjugated molecular scaffold. Inspired by nature in this way, bio-degradable highly fluorescent conjugated polymer nanoparticles for bio-medical imaging applications were then produced. The particles decompose upon exposure to ROS and the resulting small molecular degradation products are water soluble and can be excreted¹⁵⁸.

5.2.1 Future work

In future research work, various topics could be investigated with the CPN based on this dissertation. The following is a selection of the follow-up research projects that can be realised in the short-term, medium-term and long-term.

In the short term, follow up studies dedicated to the phenomenon of B-mode and PA signal change over time would be very interesting. These changes may be indicative of laser-induced vapor nanobubble formation, which increases the acoustic impedance mismatch with the surrounding medium and thus enhances the ultrasound signal, albeit transiently. This hypothesis and the influence of the CPN formulation on this phenomenon would be interesting starting points for future projects. Here, the differences in the thermal conductivity and the heat capacity of the matrix material may play a crucial role. Another future project that could be implemented in the short term is the investigation of the phototoxicity of the CPN. This is of great importance for the potential future users, since due to the high absorption coefficient of CPs a UV-induced side effect like sunburn could result.

In the medium term, changes could be made to the formulation of the CPN in order to improve its biodistribution or targeting, so that the NPs could be provided with moieties on the particle surface that allow active targeting. Different matrices could be used for the production, which are already functionalised at the PEG end with active groups such as folate or biotin in order to realise active targeting of the corresponding counterparts on cancer cells. Carboxylic acid-modified PEG-PLGA could enable in-house surface modifications that are not commercially available, for example with antibodies, proteins, affibody or peptides. Active targeting could result in higher SBR and increased sensitivity of CPNs. Since the LNC formulations showed very good optical fluorescence performance in vitro, in vivo experiments would be a reasonable next step for this technology.

In the long term, further preclinical development of the lead formulation resulting from the preceding projects would be conceivable. This would entail a subsequent in-depth evaluation of the non-clinical safety according to the ICH M3 (R2) guidelines (Non-clinical safety studies for the conduct of clinical trials in humans for drugs). Non-clinical safety studies include the evaluation of the maximum tolerated dose, the establishment of pharmacokinetic and toxicokinetic profiles and reproductive toxicity, genotoxicity, immunotoxicity and, in justified cases, carcinogenic potential. Although it is difficult to address the full spectrum of non-clinical research in an academic setting, properly designed studies in the above-mentioned areas could provide valuable information for evaluating the translatability of CPNs for future clinical application.

6 Summary

For the development of a potential in vivo diagnostic agent based on a nanoparticle suspension with both fluorescence and photoacoustic properties, it is essential to be able to meet not only in vitro and in vivo imaging performance with these two optical imaging modalities, but also the most consistent pharmaceutical quality requirements for parenteral, intravenous formulations. The novel nanodiagnostics based on PEG-PLGA or phospholipid as an envelope material for conjugated polymers were evaluated both physicochemically and chemically with respect to their biocompatibility as well as their optical and photoacoustic properties before a study in a xenograft mouse model was conducted.

In the following section, the most important results of the three publications are summarized.

1. In publication I, the influence of the PEG-PLGA structure, namely molecular weight and composition, on the encapsulation of the conjugated polymer PCPDTBT was investigated, with a focus on particle size, stability, biocompatibility and optical performance. In the optimization study, the fraction of PCPDTBT varied between 0%-50% for the three matrices used (PEG_{2kDa}-PLGA_{4kDa}, PEG_{2kDa}-PLGA_{15kDa} and PEG_{5kDa}-PLGA_{55kDa}). Based on the data obtained, a multi-variate analysis was performed to predict the hydrodynamic diameter based on the two input factors PCPDTBT content and total solids content. PEG_{2kDa}-PLGA_{15kDa} and PEG_{5kDa}-PLGA_{55kDa}, were more sensitive to changes in these factors than PEG_{2kDa}-PLGA_{4kDa}, where only the PCPDTBT content seemed to have an influence on particle size. The cytotoxicity data according to ISO10993-5 showed "slight cytotoxicity" or "mild cytotoxicity", and PCPDTBT CPNs showed a slightly higher cytotoxicity compared to pure PEG-PLGA NP. The haemocompatibility experiments revealed that, except for PEG_{2kDa}-PLGA_{15kDa}, which has low hemolytic activity, the CPN are not haemolytic regardless of composition. The in vitro optical tests showed a broadening of the absorption spectra of CPN, a strong (90 nm) redshift of the emission spectrum and 30-200 times lower PLQY compared to PCPDTBT dissolved in THF. IVIS Spectrum fluorescence in phantom imaging revealed a nearly linear signal increase over the observed concentration range (0.125-1 µg). Interestingly, PEG_{2kDa}-PLGA_{4kDa} CPNs showed slightly higher SBR

than the formulations with higher PEG-PLGA molecular weights. The PEG-PLGA structure also had an influence on the photoacoustic signal, where PEG_{2kDa}-PLGA_{4kD} CPNs showed a slightly better imaging performance.

2. In the second publication we focused on the optical performance of three CPNs of different architecture (PEG_{2kDa}-PLGA_{4kDa}, PEG_{2kDa}-DPPE and PEG_{5kDa}-PLGA_{55kDa}) in fluorescence and photoacoustic imaging in vitro and in vivo. Despite the fact that PEG_{2kDa}-DPPE CPN had a higher PLQY, it was observed that both PEG-PLGA formulations showed up to 30% higher SBR in vitro. Phantom mouse studies investigating the stability of the SBR over time indicate that the SBR reduction observed did not result from repeated excitation of the fluorophores but is thought to be due to a possible reduction of their chemical stability. After application of the QbD inspired approach to characterize the CPN suspensions, a mouse xenograft model was examined using both whole body fluorescence and photoacoustic imaging of the tumor. Fluorescence imaging revealed that PEG_{2kDa}-PLGA_{4kDa} showed higher SBR in the abdominal region 3h after application compared to the other two formulations and that PEG_{2kDa}-DPPE consistently showed higher SBR in tumor and periphery. Further in vitro experiments were performed to explain these unexpected results. SDS-PAGE revealed that PEG_{2kDa}-DPPE adsorbed the least amount of serum proteins on the NP surface, followed by PEG_{5kDa}-PLGA_{55kDa} and PEG_{2kDa}-PLGA_{4kDa}. Uptake of PEG_{2kDa}-PLGA_{4kDa} in J774A.1 macrophage like cells was higher than other systems, which may explain the initial high SBR in the abdominal region with this CPN formulation. PA in vitro studies showed possible evidence of nanobubble formation when using PEG-PLGA CPNs, which was characterised by strong PA and B-mode signals shortly after the start of the measurement, which decreased over time. In vivo, the tumor PA signal increased gradually and showed maxima after 12 hours (PEG_{2kDa}-DPPE) and after 48 hours (PEG-PLGA formulations), with PEG_{2kDa}-DPPE giving the highest signal in the tumor.
3. The focus of publication III was on the investigation of the optical performance of two different CPs, formulated as PEG-PLGA-type CPNs, in an in vivo xenograft mouse model under consideration of biodistribution, tolerability and biocompatibility/toxicology. A fully borylated F8BT (termed P4) was compared to

the commercially available PCPDTBT, both formulated into a PEG_{5kDa}-PLGA_{55kDa} matrix. Since indocyanine green (ICG) is an FDA approved dye for in vivo use in humans for NIR imaging, it was included in the in vitro studies as an aqueous solution and as a NP formulation. The PLQY of P4 (~2.3%) was similar to that of ICG+albumin and twice as high as ICG NP and about 200-fold higher than PCPDTBT NP. In the IVIS imaging phantom, ICG formulations showed concentration dependent quenching, whereas SBR of the CP suspension increased linearly with increasing concentration (12.5–100 µg/mL). Within 14 days the formulations were imaged 10 times, showing that P4 CPN was the most stable with only 12% loss of SBR, compared to PCPDTBT CPN (60%), ICG solution (100%) and ICG+albumin (44%). The physicochemical properties as well as the sterility, bacterial endotoxin tests and residual solvent level investigation revealed excellent quality of the final product, which was suitable for in vivo experiments. In vivo the SBR of the P4 CPNs was up to 5 times higher in the abdominal region, tumor and periphery compared to PCPDTBT CPNs. The tumor signal was 1.5 to 2.5 fold higher than the periphery. According to the literature, a SBR in the range of 1.1 offers sufficient discriminatory power for cancer diagnostic applications¹¹⁰.

In summary, three PCPDTBT CPN formulations with different nanoparticle architectures, i.e. two PEG-PLGA CPNs (matrix-like nanoparticles) and one phospholipid-coated CPN (core-shell type) and one P4 PEG-PLGA formulation were compared over the experimental period of the present work with respect to their fluorescence and photoacoustic imaging performance and in vivo biodistribution. Despite very similar physicochemical properties of CPN, they showed different optical and photoacoustic properties as well as different in vivo biodistribution. These formulations showed not only promising performance and good tolerability, although further development of this technology is required prior to clinical implementation.

7 References

- (1) Hong, G.; Antaris, A. L.; Dai, H. Near-Infrared Fluorophores for Biomedical Imaging. *Nat. Biomed. Eng.* **2017**, *1* (1). <https://doi.org/10.1038/s41551-016-0010>.
- (2) Hibbs, G. Believing in Seeing. *Nat. Mater.* **2014**, *13* (2), 99–99. <https://doi.org/10.1038/nmat3879>.
- (3) Fass, L. Imaging and Cancer: A Review. *Mol. Oncol.* **2008**, *2* (2), 115–152. <https://doi.org/10.1016/j.molonc.2008.04.001>.
- (4) Smith, B. R.; Gambhir, S. S. Nanomaterials for in Vivo Imaging. *Chem. Rev.* **2017**, *117* (3), 901–986. <https://doi.org/10.1021/acs.chemrev.6b00073>.
- (5) Statistisches Bundesamt. Fallpauschalenbezogene Krankenhausstatistik (DRG-Statistik) Operationen Und Prozeduren Der Vollstationären Patientinnen Und Patienten In Krankenhäusern (4-Steller). **2019**.
- (6) Dhawan, A. P.; D'Alessandro, B.; Fu, X. Optical Imaging Modalities for Biomedical Applications. *IEEE Rev. Biomed. Eng.* **2010**, *3* (12), 69–92. <https://doi.org/10.1109/RBME.2010.2081975>.
- (7) Aspect, A.; Grangier, P. Wave-Particle Duality for Single Photons. *Hyperfine Interact.* **1987**, *37*, 1–17.
- (8) Joos, G. *Theoretical Physics*, 3rd ed.; 1987.
- (9) Atkins, P.; Depaula, J.; Keeler, J. *Atkins' Physical Chemistry*, 11th ed.; 2017.
- (10) Elert, G. The Physics Hypertextbook <https://physics.info/standard/> (accessed Nov 10, 2020).
- (11) McQuarrie, D. A. *Physical Chemistry*, 2nd ed.; 2008.
- (12) Ying, X.; Barlow, N. J.; Feuston, M. H. Micro-Computed Tomography and Volumetric Imaging in Developmental Toxicology. *Reprod. Dev. Toxicol.* **2017**, 1183–1205. <https://doi.org/10.1016/B978-0-12-804239-7.00063-9>.
- (13) Reisz, J. A.; Bansal, N.; Qian, J.; Zhao, W.; Furdui, C. M. Effects of Ionizing Radiation on Biological Molecules - Mechanisms of Damage and Emerging Methods of Detection. *Antioxidants Redox Signal.* **2014**, *21* (2), 260–292. <https://doi.org/10.1089/ars.2013.5489>.
- (14) Abelha, T. F.; A. Dreiss, C.; A. Green, M.; Dailey, L. A. Conjugated Polymers as Nanoparticle Probes for Fluorescence and Photoacoustic Imaging. *J. Mater. Chem. B* **2020**, *8*, 592–606. <https://doi.org/10.1039/C9TB02582K>.
- (15) Siemens Healthcare. Understanding Medical Radiation <http://www.medicalradiation.com/types-of-medical-imaging/imaging-using-x-rays/radiography-plain-x-rays/> (accessed Aug 17, 2020).
- (16) Siemens Healthcare. Understanding Medical Radiation <http://www.medicalradiation.com/types-of-medical-imaging/imaging-using-x-rays/computed-tomography-ct/> (accessed Aug 17, 2020).

- (17) Massoud, T. F.; Gambhir, S. S. Molecular Imaging in Living Subjects: Seeing Fundamental Biological Processes in a New Light. *Genes Dev.* **2003**, *17* (5), 545–580. <https://doi.org/10.1101/gad.1047403>.
- (18) Siemens Healthcare. Understanding Medical Radiation <http://www.medicalradiation.com/types-of-medical-imaging/molecular-imaging/molecular-imaging-and-nuclear-medicine/> (accessed Aug 17, 2020).
- (19) Understanding Medical Radiation <http://www.medicalradiation.com/types-of-medical-imaging/molecular-imaging/combined-modalities/> (accessed Aug 17, 2020).
- (20) Naseri, N.; Ajorlou, E.; Asghari, F.; Pilehvar-Soltanahmadi, Y. An Update on Nanoparticle-Based Contrast Agents in Medical Imaging. *Artif. Cells, Nanomedicine Biotechnol.* **2018**, *46* (6), 1111–1121. <https://doi.org/10.1080/21691401.2017.1379014>.
- (21) Siemens Healthcare. Understanding Medical Radiation <http://www.medicalradiation.com/types-of-medical-imaging/other-types-of-medical-imaging/magnetic-resonance-imaging/> (accessed Aug 17, 2020).
- (22) Siemens Healthcare. Understanding Medical Radiation <http://www.medicalradiation.com/types-of-medical-imaging/other-types-of-medical-imaging/ultrasound-imaging/> (accessed Aug 17, 2020).
- (23) Ilnatsenka, B.; Boezaart, A. P. Ultrasound: Basic Understanding and Learning the Language. *Int. J. Shoulder Surg.* **2010**, *4* (3), 55–62. <https://doi.org/10.4103/0973-6042.76960>.
- (24) Bachmann, L.; Zzell, D. M.; Ribeiro, A. da C.; Gomes, L.; Ito, A. S. Fluorescence Spectroscopy of Biological Tissues - A Review. *Appl. Spectrosc. Rev.* **2006**, *41* (6), 575–590. <https://doi.org/10.1080/05704920600929498>.
- (25) Sharma, P.; Brown, S.; Walter, G.; Santra, S.; Moudgil, B. Nanoparticles for Bioimaging. *Adv. Colloid Interface Sci.* **2006**, *123*, 471–485. <https://doi.org/10.1016/j.cis.2006.05.026>.
- (26) Sevick-Muraca, E. M.; Houston, J. P.; Gurfinkel, M. Fluorescence-Enhanced, near Infrared Diagnostic Imaging with Contrast Agents. *Curr. Opin. Chem. Biol.* **2002**, *6* (5), 642–650. [https://doi.org/10.1016/S1367-5931\(02\)00356-3](https://doi.org/10.1016/S1367-5931(02)00356-3).
- (27) Schneider, A.; Feussner, H. *Biomedical Engineering in Gastrointestinal Surgery*, 1st ed.; 2017. <https://doi.org/10.1016/B978-0-12-803230-5.00005-1>.
- (28) Yao, J.; Wang, L. V. Sensitivity of Photoacoustic Microscopy. *Photoacoustics* **2014**, *2* (2), 87–101. <https://doi.org/10.1016/j.pacs.2014.04.002>.
- (29) He, J.; Li, C.; Ding, L.; Huang, Y.; Yin, X.; Zhang, J.; Zhang, J.; Yao, C.; Liang, M.; Pirraco, R. P.; et al. Tumor Targeting Strategies of Smart Fluorescent Nanoparticles and Their Applications in Cancer Diagnosis and Treatment. *Adv. Mater.* **2019**, *31* (40). <https://doi.org/10.1002/adma.201902409>.
- (30) Pu, K. Y.; Liu, B. Fluorescent Conjugated Polyelectrolytes for Bioimaging. *Adv. Funct. Mater.* **2011**, *21* (18), 3408–3423. <https://doi.org/10.1002/adfm.201101153>.
- (31) Wu, C.; Chiu, D. T. Highly Fluorescent Semiconducting Polymer Dots for Biology and Medicine. *Angew. Chemie - Int. Ed.* **2013**, *52* (11), 3086–3109. <https://doi.org/10.1002/anie.201205133>.

- (32) Foto-Museum Uhlingen. La cour du domaine du Gras <https://www.foto-museum-uhlingen.de/geschichte-der-fotografie/niepce/> (accessed Dec 4, 2020).
- (33) Braslavsky, S. E. Glossary of Terms Used in Photochemistry 3rd Edition: (IUPAC Recommendations 2006). *Pure Appl. Chem.* **2007**, *79* (3), 293–465. <https://doi.org/10.1351/pac200779030293>.
- (34) Miao, Q.; Pu, K. Organic Semiconducting Agents for Deep-Tissue Molecular Imaging: Second Near-Infrared Fluorescence, Self-Luminescence, and Photoacoustics. *Adv. Mater.* **2018**, *30* (49), 1–23. <https://doi.org/10.1002/adma.201801778>.
- (35) Leblond, F.; Davis, S. C.; Valdés, P. A.; Pogue, B. W. Pre-Clinical Whole-Body Fluorescence Imaging: Review of Instruments, Methods and Applications. *J. Photochem. Photobiol. B Biol.* **2010**, *98* (1), 77–94. <https://doi.org/10.1016/j.jphotobiol.2009.11.007>.
- (36) Zhu, C.; Liu, L.; Yang, Q.; Lv, F.; Wang, S. Water-Soluble Conjugated Polymers for Imaging, Diagnosis, and Therapy. *Chem. Rev.* **2012**, *112* (8), 4687–4735. <https://doi.org/10.1021/cr200263w>.
- (37) Bell, A. G. The Production of Sound by Radiant Energy. *Science.* **1881**, *2*, 242–253.
- (38) Cahen, D.; Bults, G.; Garty, H.; Malkin, S. Photoacoustics in Life Sciences. *J. Biochem. Biophys. Methods* **1980**, *3*, 293–310.
- (39) Xu, M.; Wang, L. V. Photoacoustic Imaging in Biomedicine. *Rev. Sci. Instrum.* **2006**, *77* (4). <https://doi.org/10.1063/1.2195024>.
- (40) FUJIFILM Sonosite, I. VisualSonics LAZR-X <https://www.visualsonics.com/photoacoustic-effect> (accessed Oct 5, 2020).
- (41) Pu, K.; Mei, J.; Jokerst, J. V.; Hong, G.; Antaris, A. L.; Chattopadhyay, N.; Shuhendler, A. J.; Kurosawa, T.; Zhou, Y.; Gambhir, S. S.; et al. Diketopyrrolopyrrole-Based Semiconducting Polymer Nanoparticles for in Vivo Photoacoustic Imaging. *Adv. Mater.* **2015**, *27* (35), 5184–5190. <https://doi.org/10.1002/adma.201502285>.
- (42) Liu, Y.; Teng, L.; Liu, H. W.; Xu, C.; Guo, H.; Yuan, L.; Zhang, X. B.; Tan, W. Recent Advances in Organic-Dye-Based Photoacoustic Probes for Biosensing and Bioimaging. *Sci. China Chem.* **2019**, *62* (10), 1275–1285. <https://doi.org/10.1007/s11426-019-9506-2>.
- (43) Pu, K.; Huang, J. Activatable Molecular Probes for Second Near-Infrared Fluorescence, Chemiluminescence, and Photoacoustic Imaging. *Angew. Chemie* **2020**, *59* (132), 11813–11827. <https://doi.org/10.1002/ange.202001783>.
- (44) Attia, A. B. E.; Balasundaram, G.; Moothanchery, M.; Dinish, U. S.; Bi, R.; Ntziachristos, V.; Olivo, M. A Review of Clinical Photoacoustic Imaging: Current and Future Trends. *Photoacoustics* **2019**, *16*, 100144. <https://doi.org/10.1016/j.pacs.2019.100144>.
- (45) Steinberg, I.; Huland, D. M.; Vermesh, O.; Frostig, H. E.; Tummers, W. S.; Gambhir, S. S. Photoacoustic Clinical Imaging. *Photoacoustics* **2019**, *14* (April), 77–98. <https://doi.org/10.1016/j.pacs.2019.05.001>.
- (46) Manohar, S.; Gambhir, S. S. Clinical Photoacoustic Imaging. *Photoacoustics* **2020**, *19*, 1–2.

- (47) BfArM. BfArM https://www.bfarm.de/DE/Arzneimittel/_node.html (accessed Mar 25, 2021).
- (48) Baldrick, P. Nonclinical Safety Testing of Imaging Agents, Contrast Agents and Radiopharmaceuticals. *J. Appl. Toxicol.* **2020**, 1–10. <https://doi.org/10.1002/jat.4054>.
- (49) Geisslinger, G.; Menzel, S.; Gudermann, T.; Hinz, B.; Ruth, P.; Mutschler, M. *Mutschler Arzneimittelwirkungen: Pharmakologie - Klinische Pharmakologie - Toxikologie*, 11th ed.; 2019.
- (50) World Health Organization. World Health Organization Model List of Essential Medicines. *Ment. Holist. Heal. Some Int. Perspect.* **2019**, *21*, 119–134.
- (51) Thakor, A. S.; Jokerst, J. V.; Ghanouni, P.; Campbell, J. L.; Mittra, E.; Gambhir, S. S. Clinically Approved Nanoparticle Imaging Agents. *J. Nucl. Med.* **2016**, *57* (12), 1833–1837. <https://doi.org/10.2967/jnumed.116.181362>.
- (52) Wilson, K.; Homan, K.; Emelianov, S. Biomedical Photoacoustics beyond Thermal Expansion Using Triggered Nanodroplet Vaporization for Contrast-Enhanced Imaging. *Nat. Commun.* **2012**, *3*, 610–618. <https://doi.org/10.1038/ncomms1627>.
- (53) Barth, C. W.; Gibbs, S. Fluorescence Image-Guided Surgery: A Perspective on Contrast Agent Development. **2020**, *18*. <https://doi.org/10.1117/12.2545292>.
- (54) Ballou, B.; Ernst, L. a; Waggoner, A. S. Fluorescence Imaging of Tumors in Vivo. *Curr. Med. Chem.* **2005**, *12* (7), 795–805. <https://doi.org/10.2174/0929867053507324>.
- (55) Frangioni, J. V. In Vivo Near-Infrared Fluorescence Imaging. *Curr. Opin. Chem. Biol.* **2003**, *7* (5), 626–634. <https://doi.org/10.1016/j.cbpa.2003.08.007>.
- (56) Ghoroghchian, P. P.; Therien, M. J.; Hammer, D. A. In Vivo Fluorescence Imaging: A Personal Perspective. *Wiley Interdiscip. Rev. Nanomedicine Nanobiotechnology* **2009**, *1* (2), 156–167. <https://doi.org/10.1002/wnan.7>.
- (57) Carr, J. A.; Franke, D.; Caram, J. R.; Perkinson, C. F.; Saif, M.; Askoxylakis, V.; Datta, M.; Fukumura, D.; Jain, R. K.; Bawendi, M. G.; et al. Shortwave Infrared Fluorescence Imaging with the Clinically Approved Near-Infrared Dye Indocyanine Green. *Proc. Natl. Acad. Sci.* **2018**, *115* (17), 4465–4470. <https://doi.org/10.1073/pnas.1718917115>.
- (58) Landsman, M. L.; Kwant, G.; Mook, G. A.; Zijlstra, W. G. Light-Absorbing Properties, Stability, and Spectral Stabilization of Indocyanine Green. *J. Appl. Physiol.* **1976**, *40* (4), 575–583. <https://doi.org/10.1152/jappl.1976.40.4.575>.
- (59) Philip, R.; Penzkofer, A.; Biiumler, W.; Szeimies, R. M.; Abels, C. Absorption and Fluorescence Spectroscopic Investigation of Indocyanine Green. **1996**, *96*, 137–148.
- (60) Ding, D.; Liu, J.; Feng, G.; Li, K.; Hu, Y.; Liu, B. Bright Far-Red/near-Infrared Conjugated Polymer Nanoparticles for in Vivo Bioimaging. *Small* **2013**, *9* (18), 3093–3102. <https://doi.org/10.1002/smll.201300171>.
- (61) Weber, J.; Beard, P. C.; Bohndiek, S. E. Contrast Agents for Molecular Photoacoustic Imaging. *Nat. Publ. Gr.* **2016**, *13* (8), 639–650. <https://doi.org/10.1038/nmeth.3929>.
- (62) Pu, K.; Shuhendler, A. J.; Jokerst, J. V.; Mei, J.; Gambhir, S. S.; Bao, Z.; Rao, J. Semiconducting

- Polymer Nanoparticles as Photoacoustic Molecular Imaging Probes in Living Mice. *Nat. Nanotechnol.* **2014**, *9* (3), 233–239. <https://doi.org/10.1038/nnano.2013.302>.
- (63) Li, J.; Liu, J.; Wei, C.-W.; Liu, B.; O'Donnell, M.; Gao, X. Emerging Applications of Conjugated Polymers in Molecular Imaging. *Phys. Chem. Chem. Phys.* **2013**, *15* (40), 17006–17015. <https://doi.org/10.1039/c3cp51763b>.
- (64) Chan, Y.-H.; Wu, P.-J. Semiconducting Polymer Nanoparticles as Fluorescent Probes for Biological Imaging and Sensing. *Part. Part. Syst. Charact.* **2015**, *32* (1), 11–28. <https://doi.org/10.1002/ppsc.201400123>.
- (65) Kemal, E.; Abelha, T. F.; Urbano, L.; Peters, R.; Owen, D. M.; Howes, P.; Green, M.; Dailey, L. A. Bright, near Infrared Emitting PLGA–PEG Dye-Doped CN-PPV Nanoparticles for Imaging Applications. *RSC Adv.* **2017**, *7*, 15255–15264. <https://doi.org/10.1039/c6ra25004a>.
- (66) Friend, R. H.; Gymer, R. W.; Holmes, A. B.; Burroughes, J. H.; Marks, R. N.; Taliani, C.; Bradley, D. D. C.; Dos Santos, D. A.; Brédas, J. L.; Lögdlund, M.; et al. Electroluminescence in Conjugated Polymers. *Nature* **1999**, *397* (6715), 121–128. <https://doi.org/10.1038/16393>.
- (67) Magnani, L.; Rumbles, G.; Samuel, I. D. W.; Murray, K.; Moratti, S. C.; Holmes, a. B.; Friend, R. H. Photoluminescence Studies of Chain Interactions in Electroluminescent Polymers. *Synth. Met.* **1997**, *84*, 899–900. [https://doi.org/10.1016/S0379-6779\(96\)04202-6](https://doi.org/10.1016/S0379-6779(96)04202-6).
- (68) Heeger, A.; MacDiarmid, A. G.; Shirakawa, H. The Nobel Prize in Chemistry, 2000: Conductive Polymers. *Stock. Sweden R. Swedish Acad. Sci.* **2000**, 1–16. https://doi.org/http://www.nobelprize.org/nobel_prizes/chemistry/laureates/2000/advanced-chemistryprize2000.pdf.
- (69) Moliton, A.; Hiorns, R. C. Review of Electronic and Optical Properties of Semiconducting π -Conjugated Polymers: Applications in Optoelectronics. *Polym. Int.* **2004**, *53* (10), 1397–1412. <https://doi.org/10.1002/pi.1587>.
- (70) Dou, L.; Liu, Y.; Hong, Z.; Li, G.; Yang, Y. Low-Bandgap Near-IR Conjugated Polymers/Molecules for Organic Electronics. *Chem. Rev.* **2015**, *115* (23), 12633–12665. <https://doi.org/10.1021/acs.chemrev.5b00165>.
- (71) Li, Y.; Cao, Y.; Gao, J.; Wang, D.; Yu, G.; Heeger, A. J. Electrochemical Properties of Luminescent Polymers and Polymer Light-Emitting Electrochemical Cells. *Synth. Met.* **1999**, *99* (3), 243–248. [https://doi.org/10.1016/S0379-6779\(99\)00007-7](https://doi.org/10.1016/S0379-6779(99)00007-7).
- (72) James, L. Understanding the difference between n- and p-type semiconductors <https://www.power-and-beyond.com/understanding-the-difference-between-n-and-p-type-semiconductors-a-905805/> (accessed Jul 22, 2020).
- (73) Kim, J.; Swager, T. M. Control of Conformational and Interpolymer Effects in Conjugated Polymers. *Nature* **2001**, *411* (6841), 1030–1034. <https://doi.org/10.1038/35082528>.
- (74) Rasmussen, S. C. The Early History of Polyaniline: Discovery and Origins. *An Int. J. Hist. Chem. Subst.* **2017**, *1* (12), 99–109. <https://doi.org/10.13128/substantia-30>.
- (75) Rasmussen, S. C. Conjugated and Conducting Organic Polymers : The First 150 Years. **2020**, 1412–1429. <https://doi.org/10.1002/cplu.202000325>.

- (76) Hildner, R.; Köhler, A.; Müller-Buschbaum, P.; Panzer, F.; Thelakkat, M. π -Conjugated Donor Polymers: Structure Formation and Morphology in Solution, Bulk and Photovoltaic Blends. *Adv. Energy Mater.* **2017**, *7* (16). <https://doi.org/10.1002/aenm.201700314>.
- (77) Burroughes, J. H.; Bradley, D. D. C.; Brown, A. R.; Marks, R. N.; Mackay, K.; Friend, R. H.; Burns, P. L.; Holmes, A. B. Light-Emitting Diodes Based on Conjugated Polymers. *Nature* **1990**, *347* (6293), 539–541. <https://doi.org/10.1038/347539a0>.
- (78) Crossley, D. L.; Cade, I. A.; Clark, E. R.; Escande, A.; Humphries, M. J.; King, S. M.; Vitorica-Yrezabal, I.; Ingleson, M. J.; Turner, M. L. Enhancing Electron Affinity and Tuning Band Gap in Donor-Acceptor Organic Semiconductors by Benzothiadiazole Directed C-H Borylation. *Chem. Sci.* **2015**, *6* (9), 5144–5151. <https://doi.org/10.1039/c5sc01800e>.
- (79) Akcelrud, L. Electroluminescent Polymers. *Prog. Polym. Sci.* **2003**, *28* (6), 875–962. [https://doi.org/10.1016/S0079-6700\(02\)00140-5](https://doi.org/10.1016/S0079-6700(02)00140-5).
- (80) Freeman, D. M. E.; Minotto, A.; Duffy, W.; Fallon, K. J.; McCulloch, I.; Cacialli, F.; Bronstein, H. Highly Red-Shifted NIR Emission from a Novel Anthracene Conjugated Polymer Backbone Containing Pt(II) Porphyrins. *Polym. Chem.* **2016**, *7* (3), 722–730. <https://doi.org/10.1039/c5py01473e>.
- (81) Braun, D. Semiconducting Polymer LEDs. *Mater. Today* **2002**, *5* (6), 32–39. [https://doi.org/10.1016/S1369-7021\(02\)00637-5](https://doi.org/10.1016/S1369-7021(02)00637-5).
- (82) Braun, D.; Heeger, A. J.; Braun, D.; Heeger, A. J. Visible Light Emission from Semiconducting Polymer Diodes Visible Light Emission from Semiconducting Polymer Diodes. **1991**, *1982* (May 2013). <https://doi.org/10.1063/1.105039>.
- (83) Günes, S.; Neugebauer, H.; Sariciftci, N. S. Conjugated Polymer-Based Organic Solar Cells. *Chem. Rev.* **2007**, *107* (4), 1324–1338. <https://doi.org/10.1021/cr050149z>.
- (84) Yi, Y.; Liu, G.; Jin, Z.; Feng, D. The Use of Conducting Polyaniline as Corrosion Inhibitor for Mild Steel in Hydrochloric Acid. *Int. J. Electrochem. Sci.* **2013**, *8* (3), 3540–3550.
- (85) Costa, C. V.; Gama, L. I. L. M.; Damasceno, N. O.; Assis, A. M. L.; Soares, W. M. G.; Silva, R. C.; Tonholo, J.; Ribeiro, A. S. Bilayer Systems Based on Conjugated Polymers for Fluorescence Development of Latent Fingerprints on Stainless Steel. *Synth. Met.* **2020**, *262* (December 2019). <https://doi.org/10.1016/j.synthmet.2020.116347>.
- (86) Heeger, P. S.; Heeger, A. J. Making Sense of Polymer-Based Biosensors. **1999**, *96* (22), 12219–12221.
- (87) Sivakumar, G.; Pratyusha, T.; Shen, W.; Gupta, D. Performance of Donor-Acceptor Copolymer Materials PCPDTBT and PCDTBT with Poly Hexyl Thiophene Polymer in a Ternary Blend. *Mater. Today Proc.* **2017**, *4* (4), 5060–5066. <https://doi.org/10.1016/j.matpr.2017.04.114>.
- (88) Schulz, G. L.; Fischer, F. S. U.; Trefz, D.; Melnyk, A.; Hamidi-Sakr, A.; Brinkmann, M.; Andrienko, D.; Ludwigs, S. The PCPDTBT Family: Correlations between Chemical Structure, Polymorphism, and Device Performance. *Macromolecules* **2017**, *50* (4), 1402–1414. <https://doi.org/10.1021/acs.macromol.6b01698>.
- (89) Martin, E. J. J.; Bérubé, N.; Provencher, F.; Côté, M.; Silva, C.; Doorn, S. K.; Grey, J. K. Resonance Raman Spectroscopy and Imaging of Push–Pull Conjugated Polymer–Fullerene

- Blends. *J. Mater. Chem. C* **2015**, *3* (23), 6058–6066. <https://doi.org/10.1039/C5TC00847F>.
- (90) Yoon, J.; Kwag, J.; Shin, T. J.; Park, J. J.; Lee, Y. M. Y.; Park, J. J.; Heo, J.; Joo, C.; Park, T. J.; Yoo, P. J.; et al. Nanoparticles of Conjugated Polymers Prepared from Phase-Separated Films of Phospholipids and Polymers for Biomedical Applications. *Adv. Mater.* **2014**, *26* (26), 4559–4564. <https://doi.org/10.1002/adma.201400906>.
- (91) Russell, G.; Kingsborough, R.; Waller, D.; Zhu, Z. Polymers with Low Band Gaps and High Charge Mobility. US 200700 14939A1, 2007.
- (92) Rao, J.; Pu, K.; Shuhendler, A. Semiconducting Nanoparticles as Photoacoustic Molecular Imaging Probes. US 2015/0031996 A1, 2015.
- (93) Crossley, D. L.; Urbano, L.; Neumann, R.; Bourke, S.; Jones, J.; Dailey, L. A.; Green, M.; Humphries, M. J.; King, S. M.; Turner, M. L.; et al. Post-Polymerization C-H Borylation of Donor-Acceptor Materials Gives Highly Efficient Solid State Near-Infrared Emitters for Near-IR-OLEDs and Effective Biological Imaging. *ACS Appl. Mater. Interfaces* **2017**, *9* (34), 28243–28249. <https://doi.org/10.1021/acsami.7b08473>.
- (94) INGLESÓN, M. J.; TURNER, M. L.; Crossley, D. L. Borylated Compounds. WO 2015/189627 A1, 2015.
- (95) Neumann, P. R.; Crossley, D.; Turner, M.; Ingleson, M.; Green, M.; Rao, J.; Dailey, L. A. In Vivo Optical Performance of a New Class of near Infrared-Emitting Conjugated Polymers: Borylated PF8-BT. *ACS Appl. Mater. Interfaces* **2019**, *11* (50), 46525–46535. <https://doi.org/10.1021/acsami.9b17022>.
- (96) Soares, S.; Sousa, J.; Pais, A.; Vitorino, C. Nanomedicine: Principles, Properties, and Regulatory Issues. *Front. Chem.* **2018**, *6* (AUG), 1–15. <https://doi.org/10.3389/fchem.2018.00360>.
- (97) Mittal, B. QbD: A Welcome Evolution Only. In *How to Integrate Quality by Efficient Design (QbED) in Product Development*; 2020; pp 87–114. <https://doi.org/10.1016/B978-0-12-816813-4.00004-0>.
- (98) Beg, S.; Hasnain, M. S.; Rahman, M.; Swain, S. Introduction to Quality by Design (QbD): Fundamentals, Principles, and Applications. In *Pharmaceutical Quality by Design*; Elsevier Inc., 2019; pp 1–17. <https://doi.org/10.1016/b978-0-12-815799-2.00001-0>.
- (99) Schlindwein, W. S.; Gibson, M. Introduction to Quality by Design (QbD). In *Pharmaceutical Quality by Design: A Practical Approach*; 2017; pp 1–9. <https://doi.org/10.1002/9781118895238>.
- (100) ICH-Q8(R2). ICH Guideline Q8 (R2) on Pharmaceutical Development EMA/CHMP/ICH/167068/2004. **2009**, *8* (June).
- (101) FDA. Guidance for Industry - Quality Systems Approach to Pharmaceutical CGMP Regulations. **2006**, No. September, 32. <https://doi.org/http://www.fda.gov/CDER/guidance/6419fnl.pdf>.
- (102) Rapalli, V. K.; Khosa, A.; Singhvi, G.; Girdhar, V.; Jain, R.; Dubey, S. K. Application of QbD Principles in Nanocarrier-Based Drug Delivery Systems. In *Pharmaceutical Quality by Design*; Elsevier Inc., 2019; pp 255–296. <https://doi.org/10.1016/b978-0-12-815799-2.00014-9>.
- (103) ICH. *ICH HARMONISED TRIPARTITE GUIDELINE Quality Risk Management Q9*; 2005.

- (104) ICH. *ICH HARMONISED TRIPARTITE GUIDELINE Pharmaceutical Quality System Q10 Guideline*; 2008.
- (105) Agdeppa, E. D.; Spilker, M. E. A Review of Imaging Agent Development. *AAPS J.* **2009**, *11* (2), 286–299. <https://doi.org/10.1208/s12248-009-9104-5>.
- (106) Dailey, L. A. Pharmaceutical Quality by Design in Academic Nanomedicine Research: Stifling Innovation or Creativity through Constraint? *J. Interdiscip. Nanomedicine* **2018**, *3* (4), 175–182. <https://doi.org/10.1002/jin2.52>.
- (107) Park, S. Y.; Kang, Z.; Thapa, P.; Jin, Y. S.; Park, J. W.; Lim, H. J.; Lee, J. Y.; Lee, S. W.; Seo, M. H.; Kim, M. S.; et al. Development of Sorafenib Loaded Nanoparticles to Improve Oral Bioavailability Using a Quality by Design Approach. *Int. J. Pharm.* **2019**, *566* (March), 229–238. <https://doi.org/10.1016/j.ijpharm.2019.05.064>.
- (108) Kurmi, B. Das; Paliwal, R.; Paliwal, S. R. Dual Cancer Targeting Using Estrogen Functionalized Chitosan Nanoparticles Loaded with Doxorubicin-Estrone Conjugate: A Quality by Design Approach. *Int. J. Biol. Macromol.* **2020**, *164*, 2881–2894. <https://doi.org/10.1016/j.ijbiomac.2020.08.172>.
- (109) Gurumukhi, V. C.; Bari, S. B. Fabrication of Efavirenz Loaded Nano-Formulation Using Quality by Design (QbD) Based Approach: Exploring Characterizations and in Vivo Safety. *J. Drug Deliv. Sci. Technol.* **2020**, *56* (November 2019), 101545. <https://doi.org/10.1016/j.jddst.2020.101545>.
- (110) Hutteman, M.; Mieog, J. S. D.; Vorst, J. R. van der; Liefers, G.-J.; Putter, H.; Löwik, C. W. G. M.; Frangioni, J. V.; Velde, C. J. H. van de; Vahrmeijer, A. L. Randomized, Double-Blind Comparison of Indocyanine Green with or without Albumin Premixing for near-Infrared Fluorescence imaging of Sentinel Lymph Nodes in Breast Cancer Patients. *Breast Cancer Res Treat* **2011**, *127* (1), 163–170. <https://doi.org/10.1038/jid.2014.371>.
- (111) Kuehne, A. J. C. Conjugated Polymer Nanoparticles toward In Vivo Theranostics - Focus on Targeting, Imaging, Therapy, and the Importance of Clearance. *Adv. Biosyst.* **2017**, No. August, 1700100. <https://doi.org/10.1002/adbi.201700100>.
- (112) Li, J.; Rao, J.; Pu, K. Recent Progress on Semiconducting Polymer Nanoparticles for Molecular Imaging and Cancer Phototherapy. *Biomaterials* **2018**, *155*, 217–235. <https://doi.org/10.1016/j.biomaterials.2017.11.025>.
- (113) Jiang, Y.; Upputuri, P. K.; Xie, C.; Zeng, Z.; Sharma, A.; Zhen, X.; Li, J.; Huang, J.; Pramanik, M.; Pu, K. Metabolizable Semiconducting Polymer Nanoparticles for Second Near-Infrared Photoacoustic Imaging. *Adv. Mater.* **2019**, *31* (11), 1–9. <https://doi.org/10.1002/adma.201808166>.
- (114) Tuncel, D. π -Conjugated Nanostructured Materials: Preparation, Properties and Photonic Applications. *Nanoscale Adv.* **2019**, *1* (1), 19–33. <https://doi.org/10.1039/c8na00108a>.
- (115) Grey, J. K.; Kim, D. Y.; Norris, B. C.; Miller, W. L.; Barbara, P. F. Size-Dependent Spectroscopic Properties of Conjugated Polymer Nanoparticles. *J. Phys. Chem. B* **2006**, *110* (51), 25568–25572. <https://doi.org/10.1021/jp065990a>.
- (116) Pecher, J.; Mecking, S. Nanoparticles of Conjugated Polymers. *Chem. Rev.* **2010**, *110* (10), 6260–6279. <https://doi.org/10.1021/cr100132y>.

- (117) Qian, C. G.; Zhu, S.; Feng, P. J.; Chen, Y. L.; Yu, J. C.; Tang, X.; Liu, Y.; Shen, Q. D. Conjugated Polymer Nanoparticles for Fluorescence Imaging and Sensing of Neurotransmitter Dopamine in Living Cells and the Brains of Zebrafish Larvae. *ACS Appl. Mater. Interfaces* **2015**, *7* (33), 18581–18589. <https://doi.org/10.1021/acsami.5b04987>.
- (118) Li, D. D.; Wang, J. X.; Ma, Y.; Qian, H. S.; Wang, D.; Wang, L.; Zhang, G.; Qiu, L.; Wang, Y. C.; Yang, X. Z. A Donor-Acceptor Conjugated Polymer with Alternating Isoindigo Derivative and Bithiophene Units for Near-Infrared Modulated Cancer Thermo-Chemotherapy. *ACS Appl. Mater. Interfaces* **2016**, *8* (30), 19312–19320. <https://doi.org/10.1021/acsami.6b05495>.
- (119) Xu, L.; Cheng, L.; Wang, C.; Peng, R.; Liu, Z. Conjugated Polymers for Photothermal Therapy of Cancer. *Polym. Chem.* **2014**, *5* (5), 1573–1580. <https://doi.org/10.1039/c3py01196h>.
- (120) Sarkar, S.; Levi-Polyachenko, N. Conjugated Polymer Nano-Systems for Hyperthermia, Imaging and Drug Delivery. *Adv. Drug Deliv. Rev.* **2020**, *163*, 40–64. <https://doi.org/10.1016/j.addr.2020.01.002>.
- (121) Feng, G.; Fang, Y.; Liu, J.; Geng, J.; Ding, D.; Liu, B. Multifunctional Conjugated Polymer Nanoparticles for Image-Guided Photodynamic and Photothermal Therapy. *Small* **2017**, *13* (3), 1–12. <https://doi.org/10.1002/sml.201602807>.
- (122) Xu, X.; Liu, R.; Li, L. Nanoparticles Made of π -Conjugated Compounds Targeted for Chemical and Biological Applications. *Chem. Commun.* **2015**, *51* (94), 16733–16749. <https://doi.org/10.1039/c5cc06439b>.
- (123) Cheng, J.; Teply, B. A.; Sherifi, I.; Sung, J.; Luther, G.; Gu, F. X.; Levy-Nissenbaum, E.; Radovic-Moreno, A. F.; Langer, R.; Farokhzad, O. C. Formulation of Functionalized PLGA-PEG Nanoparticles for in Vivo Targeted Drug Delivery. *Biomaterials* **2007**, *28* (5), 869–876. <https://doi.org/10.1016/j.biomaterials.2006.09.047>.
- (124) Feng, L.; Zhu, C.; Yuan, H.; Liu, L.; Lv, F.; Wang, S. Conjugated Polymer Nanoparticles: Preparation, Properties, Functionalization and Biological Applications. *Chem. Soc. Rev. Chem. Soc. Rev* **2013**, *42* (42), 6620–6633. <https://doi.org/10.1039/c3cs60036j>.
- (125) Shim, M. S.; Kwon, Y. J. Stimuli-Responsive Polymers and Nanomaterials for Gene Delivery and Imaging Applications. *Adv. Drug Deliv. Rev.* **2012**, *64* (11), 1046–1059. <https://doi.org/10.1016/j.addr.2012.01.018>.
- (126) Fedatto Abelha, T.; Phillips, T. W.; Bannock, J. H.; Nightingale, A.; Dreiss, C. A.; Kemal, E.; Urbano, L.; de Mello, J. C.; Green, M.; Dailey, L. A. Bright Conjugated Polymer Nanoparticles Containing a Biodegradable Shell Produced at High Yields and with Tuneable Optical Properties by a Scalable Microfluidic Device. *Nanoscale* **2017**, *9* (2009), 2009–2019.
- (127) Urbano, L.; Clifton, L.; Ku, H. K.; Kendall-Troughton, H.; Vandera, K. K. A.; Matarese, B. F. E.; Abelha, T.; Li, P.; Desai, T.; Dreiss, C. A.; et al. Influence of the Surfactant Structure on Photoluminescent π -Conjugated Polymer Nanoparticles: Interfacial Properties and Protein Binding. *Langmuir* **2018**, *34* (21), 6125–6137. <https://doi.org/10.1021/acs.langmuir.8b00561>.
- (128) Ahmad Khanbeigi, R.; Abelha, T. F.; Woods, A.; Rastoin, O.; Harvey, R. D.; Jones, M. C.; Forbes, B.; Green, M. A.; Collins, H.; Dailey, L. A. Surface Chemistry of Photoluminescent F8BT Conjugated Polymer Nanoparticles Determines Protein Corona Formation and Internalization by Phagocytic Cells. *Biomacromolecules* **2015**, *16* (3), 733–742. <https://doi.org/10.1021/bm501649y>.

- (129) Partikel, K.; Korte, R.; Stein, N. C.; Mulac, D.; Herrmann, F. C.; Humpf, H.; Langer, K. Effect of Nanoparticle Size and PEGylation on the Protein Corona of PLGA Nanoparticles. *Eur. J. Pharm. Biopharm.* **2019**, *141* (May), 70–80. <https://doi.org/10.1016/j.ejpb.2019.05.006>.
- (130) Konstantinos Avgoustakis. Pegylated Poly(Lactide) and Poly(Lactide-Co-Glycolide) Nanoparticles: Preparation, Properties and Possible Applications in Drug Delivery. *Curr. Drug Deliv.* **2004**, *1* (4), 13. <https://doi.org/10.2174/1567201043334605>
- (131) Kamaly, N.; Xiao, Z.; Valencia, P. M.; Radovic-Moreno, A. F.; Farokhzad, O. C. Targeted Polymeric Therapeutic Nanoparticles: Design, Development and Clinical Translation. *Chem. Soc. Rev.* **2012**, *41* (7), 2971–3010. <https://doi.org/10.1039/c2cs15344k>.
- (132) Zhang, K.; Tang, X.; Zhang, J.; Lu, W.; Lin, X.; Zhang, Y.; Tian, B.; Yang, H.; He, H. PEG-PLGA Copolymers: Their Structure and Structure-Influenced Drug Delivery Applications. *J. Control. Release* **2014**, *183* (1), 77–86. <https://doi.org/10.1016/j.jconrel.2014.03.026>.
- (133) Keles, H.; Naylor, A.; Clegg, F.; Sammon, C. Investigation of Factors Influencing the Hydrolytic Degradation of Single PLGA Microparticles. *Polym. Degrad. Stab.* **2015**, *119*, 228–241. <https://doi.org/10.1016/j.polymdegradstab.2015.04.025>.
- (134) Moore, T. L.; Rodriguez-Lorenzo, L.; Hirsch, V.; Balog, S.; Urban, D.; Jud, C.; Rothen-Rutishauser, B.; Lattuada, M.; Petri-Fink, A. Nanoparticle Colloidal Stability in Cell Culture Media and Impact on Cellular Interactions. *Chem. Soc. Rev.* **2015**, *44* (17), 6287–6305. <https://doi.org/10.1039/C4CS00487F>.
- (135) Schöttler, S.; Becker, G.; Winzen, S.; Steinbach, T.; Mohr, K.; Landfester, K.; Mailänder, V.; Wurm, F. R. Protein Adsorption Is Required for Stealth Effect of Poly(Ethylene Glycol)- and Poly(Phosphoester)- Coated Nanocarriers. *Nat. Nanotechnol.* **2016**, *11*, 372–377. <https://doi.org/10.1038/nnano.2015.330>.
- (136) Chrastina, A.; Massey, K. A.; Schnitzer, J. E. Overcoming in Vivo Barriers to Targeted Nanodelivery. *Wiley Interdiscip. Rev. Nanomedicine Nanobiotechnology* **2011**, *3* (4), 421–437. <https://doi.org/10.1002/wnan.143>.
- (137) Garnett, M. C.; Kallinteri, P. Nanomedicines and Nanotoxicology: Some Physiological Principles. *Occup. Med.* **2006**, *56* (5), 307–311. <https://doi.org/10.1093/occmed/kql052>.
- (138) Ritz, S.; Schöttler, S.; Kotman, N.; Baier, G.; Musyanovych, A.; Kuharev, J.; Landfester, K.; Schild, H.; Jahn, O.; Tenzer, S.; et al. Protein Corona of Nanoparticles: Distinct Proteins Regulate the Cellular Uptake. *Biomacromolecules* **2015**, *16* (4), 1311–1321. <https://doi.org/10.1021/acs.biomac.5b00108>.
- (139) Nag, O. K.; Awasthi, V. Surface Engineering of Liposomes for Stealth Behavior. *Pharmaceutics* **2013**, *5*, 542–569. <https://doi.org/10.3390/pharmaceutics5040542>.
- (140) Gamucci, O.; Bertero, A.; Gagliardi, M.; Bardi, G. Biomedical Nanoparticles: Overview of Their Surface Immune-Compatibility. *Coatings* **2014**, *4* (1), 139–159. <https://doi.org/10.3390/coatings4010139>.
- (141) Choi, H. S.; Liu, W.; Misra, P.; Tanaka, E.; Zimmer, J. P.; Ipe, B.; Bawendi, M. G.; Frangioni, J. V. Renal Clearance of Nanoparticles. *Nat. Biotechnol.* **2009**, *25* (10), 1165–1170.

<https://doi.org/10.1038/nbt1340>.

- (142) Blanco, E.; Shen, H.; Ferrari, M. Principles of Nanoparticle Design for Overcoming Biological Barriers to Drug Delivery. *Nat. Biotechnol.* **2015**, *33* (9), 941–951. <https://doi.org/10.1038/nbt.3330>.
- (143) Wu, C.; Szymanski, C.; McNeill, J. Preparation and Encapsulation of Highly Fluorescent Conjugated Polymer Nanoparticles. *Langmuir* **2006**, *22* (7), 2956–2960. <https://doi.org/10.1021/la060188l>.
- (144) Wang, H.; Li, X.; Tse, B. W.; Yang, H.; Thorling, C. A.; Liu, Y.; Touraud, M.; Chouane, J. B.; Liu, X.; Roberts, M. S.; et al. Theranostics Indocyanine Green-Incorporating Nanoparticles for Cancer Theranostics. *Theranostics* **2018**, *8* (5), 1227–1242. <https://doi.org/10.7150/thno.22872>.
- (145) Sun, K.; Chen, H.; Wang, L.; Yin, S.; Wang, H.; Xu, G.; Chen, D.; Zhang, X.; Wu, C.; Qin, W. Size-Dependent Property and Cell Labeling of Semiconducting Polymer Dots. *ACS Appl. Mater. Interfaces* **2014**, *6* (13), 10802–10812. <https://doi.org/10.1021/am502733n>.
- (146) Zhu, H.; Fang, Y.; Zhen, X.; Wei, N.; Gao, Y.; Luo, K. Q.; Xu, C.; Duan, H.; Ding, D.; Chen, P.; et al. Multilayered Semiconducting Polymer Nanoparticles with Enhanced NIR Fluorescence for Molecular Imaging in Cells, Zebrafish and Mice. *Chem. Sci.* **2016**, *7* (8), 5118–5125. <https://doi.org/10.1039/C6SC01251E>.
- (147) Pu, K.; Mei, J.; Jokerst, J. V.; Hong, G.; Antaris, A. L.; Chattopadhyay, N.; Shuhendler, A. J.; Kurosawa, T.; Zhou, Y.; Gambhir, S. S.; et al. Diketopyrrolopyrrole-Based Semiconducting Polymer Nanoparticles for in Vivo Photoacoustic Imaging. *Adv. Mater.* **2015**, *27* (35), 5184–5190. <https://doi.org/10.1002/adma.201502285>.
- (148) Modicano, P.; Neumann, P. R.; Schüller, M.; Holthof, J.; Kyrilis, F. L.; Hamdi, F.; Kastritis, P. L.; Mäder, K.; Ann Dailey, L. Enhanced Optical Imaging Properties of Lipid Nanocapsules as Vehicles for Fluorescent Conjugated Polymers. *Eur. J. Pharm. Biopharm.* **2020**, *154* (July), 297–308. <https://doi.org/10.1016/j.ejpb.2020.07.017>.
- (149) Neumann, P. R.; Erdmann, F.; Holthof, J.; Hädrich, G.; Green, M.; Rao, J.; Dailey, L. A. Different PEG-PLGA Matrices Influence In Vivo Optical/Photoacoustic Imaging Performance and Biodistribution of NIR-Emitting π -Conjugated Polymer Contrast Agents. *Adv. Healthc. Mater.* **2020**, *2001089*, 1–13. <https://doi.org/10.1002/adhm.202001089>.
- (150) Abelha, T. F.; Neumann, P. R.; Holthof, J.; Dreiss, C. A.; Alexander, C.; Green, M.; Dailey, L. A. Low Molecular Weight PEG–PLGA Polymers Provide a Superior Matrix for Conjugated Polymer Nanoparticles in Terms of Physicochemical Properties, Biocompatibility and Optical/Photoacoustic Performance. *J. Mater. Chem. B* **2019**. <https://doi.org/10.1039/c9tb00937j>.
- (151) Neumann, P. R.; Crossley, D. L.; Turner, M.; Ingleson, M.; Green, M.; Rao, J.; Dailey, L. A. In Vivo Optical Performance of a New Class of Near-Infrared-Emitting Conjugated Polymers: Borylated PF8-BT. *ACS Appl. Mater. Interfaces* **2019**, *11* (50), 46525–46535. <https://doi.org/10.1021/acsami.9b17022>.
- (152) Repenko, T.; Rix, A.; Nedilko, A.; Rose, J.; Hermann, A.; Vinokur, R.; Moli, S.; Cao-Milà, R.; Mayer, M.; von Plessen, G.; et al. Strong Photoacoustic Signal Enhancement by Coating Gold Nanoparticles with Melanin for Biomedical Imaging. *Adv. Funct. Mater.* **2018**, *28* (7), 1–8.

- (153) Xie, C.; Zhou, W.; Zeng, Z.; Fan, Q.; Pu, K. Grafted Semiconducting Polymer Amphiphiles for Multimodal Optical Imaging and Combination Phototherapy. *Chem. Eng. News* **2020**, 1–18. <https://doi.org/10.1021/cen-v068n020.p042>.
- (154) Zhen, X.; Feng, X.; Xie, C.; Zheng, Y.; Pu, K. Surface Engineering of Semiconducting Polymer Nanoparticles for Amplified Photoacoustic Imaging. *Biomaterials* **2017**, *127*, 97–106. <https://doi.org/10.1016/j.biomaterials.2017.03.003>.
- (155) Li, J.; Pu, K. Semiconducting Polymer Nanomaterials as Near-Infrared Photoactivatable Protherapeutics for Cancer. *Acc. Chem. Res.* **2020**, *53* (4), 752–762. <https://doi.org/10.1021/acs.accounts.9b00569>.
- (156) Li, J.; Huang, J.; Lyu, Y.; Huang, J.; Jiang, Y.; Xie, C.; Pu, K. Photoactivatable Organic Semiconducting Pro-Nanoenzymes. *J. Am. Chem. Soc.* **2019**, *141* (9), 4073–4079. <https://doi.org/10.1021/jacs.8b13507>.
- (157) Li, J.; Xie, C.; Huang, J.; Jiang, Y.; Miao, Q.; Pu, K. Semiconducting Polymer Nanoenzymes with Photothermic Activity for Enhanced Cancer Therapy. *Angew. Chemie - Int. Ed.* **2018**, *57* (15), 3995–3998. <https://doi.org/10.1002/anie.201800511>.
- (158) Repenko, T.; Rix, A.; Ludwanowski, S.; Go, D.; Kiessling, F.; Lederle, W.; Kuehne, A. J. C. Bio-Degradable Highly Fluorescent Conjugated Polymer Nanoparticles for Bio-Medical Imaging Applications. *Nat. Commun.* **2017**, *8* (1), 470.

8 Appendix

Martin-Luther-Universität Halle-Wittenberg
Naturwissenschaftliche Fakultät I
- Biowissenschaften-

Eidesstattliche Erklärung / Declaration under Oath

Ich erkläre gemäß § 5 der Promotionsordnung der Naturwissenschaftlichen Fakultäten I, II & III der Martin-Luther-Universität Halle-Wittenberg an Eides statt, dass ich die Arbeit selbstständig und ohne fremde Hilfe verfasst, keine anderen als die von mir angegebenen Quellen und Hilfsmittel benutzt und die den benutzten Werken wörtlich oder inhaltlich entnommenen Stellen als solche kenntlich gemacht habe.

Weiterhin erkläre ich, dass ich mich mit der vorliegenden Dissertationsarbeit erstmals um die Erlangung eines Doktorgrades bewerbe.

I declare according to § 5 of "Promotionsordnung der Naturwissenschaftlichen Fakultäten I, II & III der Martin-Luther-Universität Halle-Wittenberg" under penalty of perjury that this thesis is my own work entirely and has been written without any help from other people. I used only the sources mentioned and included all the citations correctly both in word or content. Furthermore, I declare that this thesis has not been submitted to another faculty. This is my first application for a PhD title.

Datum / Date

Unterschrift des Antragstellers / *Signature of the applicant*

Apotheker Paul Robert Neumann

Persönliche Daten

Geburtsdatum: 08.04.1990
Geburtsort: 06217 Merseburg
Staatsangehörigkeit: Bundesrepublik Deutschland
Anschrift:

Bildungsgang

Schulische Bildung: 08/2002 – 07/2009 Abitur am Domgymnasium Merseburg

Berufliche Bildung: 10/2010 – 03/2015 – Studium der Pharmazie an der
Universität Leipzig

09/2012 – 01/2013 Auslandssemester an der Universität
Basel

05/2015 – 10/2015 Forschungsaufenthalt am King's
College London zur Anfertigung der Diplomarbeit

05/2016 Approbation zum Apotheker

seit 07/2016 Promotion (Dr.rer.nat.) in der Arbeitsgruppe
Biopharmazie an der Martin-Luther-Universität Halle-
Wittenberg

*Thema: Quality-by-Design inspired formulation of
conjugated polymer nanoparticles as contrast agents and
the assessment of optical imaging performance and
biodistribution*

Betreuung: Prof. Dr. Lea Ann Dailey

01/2018-03/2018 Forschungsaufenthalt Stanford University

Paul Robert Neumann

Veröffentlichungen

Paul Robert Neumann, Frank Erdmann, Joost Holthof, Gabriela Hädrich, Mark Green
Jianghong Rao, Lea Ann Dailey

Different PEG-PLGA Matrices Influence In Vivo Optical/Photoacoustic Imaging Performance and Biodistribution of NIR-Emitting π -Conjugated Polymer Contrast Agents. Aug. 2020 - Advanced Healthcare Materials

Ayasha Patela, Natalja Redingerde, Adrian Richter, Arcadia Woods, Paul Robert Neumann, Gemma Keegan, Nick Childerhouse, Peter Imming, Ulrich E. Schaible, Ben Forbes, Lea Ann Dailey

In vitro and in vivo antitubercular activity of benzothiazinone-loaded human serum albumin nanocarriers designed for inhalation. Aug. 2020 - Journal of Controlled

Paola Modicano, Paul Robert Neumann, Moritz Schüller, Joost Holthof, Fotis L. Kyrilis, Farzad Hamdi, Panagiotis L. Kastiris, Karsten Mäder, Lea Ann Dailey

Enhanced optical imaging properties of lipid nanocapsules as vehicles for fluorescent conjugated polymers. Jul. 2020 - European Journal of Pharmaceutics and Biopharmaceutics

Paul Robert Neumann, Daniel L. Crossley, Michael Turner, Michael Ingleson, Mark Green, Jianghong Rao, Lea Ann Dailey

In vivo optical performance of a new class of near infrared-emitting conjugated polymers: borylated PF8-BT. Nov. 2019 - ACS Applied Materials & Interfaces

Thais Fedatto Abelha, Paul Robert Neumann, Joost Holthof, Cécile A. Dreiss, Cameron Alexander, Mark Green, Lea Ann Dailey

Low molecular weight PEG-PLGA polymers provide a superior matrix for conjugated polymer nanoparticles in terms of physicochemical properties, biocompatibility and optical/photoacoustic performance. Jul. 2019 - Journal of Materials Chemistry B

Daniel L. Crossley, Laura Urbano, Robert Neumann, Struan Bourke, Jennifer Jones, Lea Ann Dailey, Mark Green, Martin J. Humphries, Simon M. King, Michael L. Turner, Michael J. Ingleson

Post-Polymerization C-H Borylation of Donor-Acceptor Materials Gives Highly Efficient Solid State Near-Infrared Emitters for NIR-OLEDs and Effective Biological Imaging. Aug 2017 - ACS Applied Materials & Interfaces

Konferenzbeiträge:

Optical imaging with borylated polyfluorene nanoparticles. Particle Based Materials Symposium, September 2019, Ulm - poster (awarded with poster prize)

Optical imaging with borylated polyfluorene nanoparticles. BioNanoMed, April 2019, Graz - oral presentation

A new optical imaging probe - bright and almost unbleachable Controlled Release Society Local Chapter Meeting, March 2019, Leipzig, Germany - poster

Borylated polyfluorenes are highly stable optical imaging probes. Molecular Imaging Symposium, MoBi. December 2018 at Max-Planck-Institute for Experimental Medicine, Göttingen - poster

Biodegradation of PEG-PLGA-based nanodiagnostics containing π -conjugated polymers as optical imaging agents. April 2017 - Journal of Interdisciplinary Nanomedicine, John Wiley & Sons, Ltd. European Conference on Nanomedicine at King's College London, 2017 – poster

Danksagung

An dieser Stelle möchte ich mich herzlich bei all jenen Personen bedanken, welche mich während der Anfertigung dieser Arbeit unterstützt haben.

Prof. Lea Ann Dailey, dir danke ich für die Überlassung des sehr interessanten und ergiebigen Themas, die hervorragende wissenschaftliche Betreuung, dein konstruktives Feedback, deine gute Erreichbarkeit, deine Ermunterung zur aktiven Teilnahme an Konferenzen, deiner Unterstützung bei der DAAD-Bewerbung und für die vielen schönen Arbeitsgruppentreffen am Donnerstagabend.

Ich danke der gesamten Arbeitsgruppe Biopharmazie, Moritz Schüller, Paola Modicano, Gabriela Hädrich, Julia Kollan, Antje Harbach, Feng Li, Richard Harvey und Lysann Tietze für die schöne Zeit und die gute Zusammenarbeit.

Ich danke Prof. Dr. Karsten Mäder für die Kooperation, für den unkomplizierten Zugang zu Messgräten und Gesprächen. Ich danke Dr. Henrike Lucas für die hilfreichen fachlichen Gespräche über Fluoreszenzbildgebung und Mausanatomie. Ich danke Tom Wersig und Erik Lehner für die gute Starthilfe zu Beginn meiner Promotionszeit.

Ich danke Prof. Jianghong Rao für die Möglichkeit, dass ich in seiner Arbeitsgruppe einen 3-monatigen Forschungsaufenthalt an der Stanford University durchführen konnte. Seiner Arbeitsgruppe, vor allem Min Chen, Xianchuang Zheng, Liyang Cui, Jinghang Xie, Zixin Chen und Antonio Benayas möchte ich danken, dass sie diesen Aufenthalt zu einer sehr produktiven und angenehmen Zeit machten.

Ich danke Joost Holthof für die gute Kooperation und Hilfe bei der Photoakustischen Bildgebung.

Ich danke Dr. Frank Erdmann für die tatkräftige Hilfe bei der Durchführung der SDS-Page sowie für die wissenschaftlichen und persönlichen Gespräche.

Ich danke Dr. Peter Lindemann für die tatkräftige und unkomplizierte Unterstützung bei der SPME GC/MS Messung.

Ich danke dem DAAD für die Gewährung eines Doktorandenstipendiums.

Ich danke Annegret Jahn für ihre kreative Umsetzung einiger Abbildungen.

Ich danke meinen Eltern und meiner Großmutter für ihr Vertrauen und ihre umfangliche Unterstützung sowie meiner Frau für die Motivation und Aufmunterung in vielen Momenten der letzten Jahre.